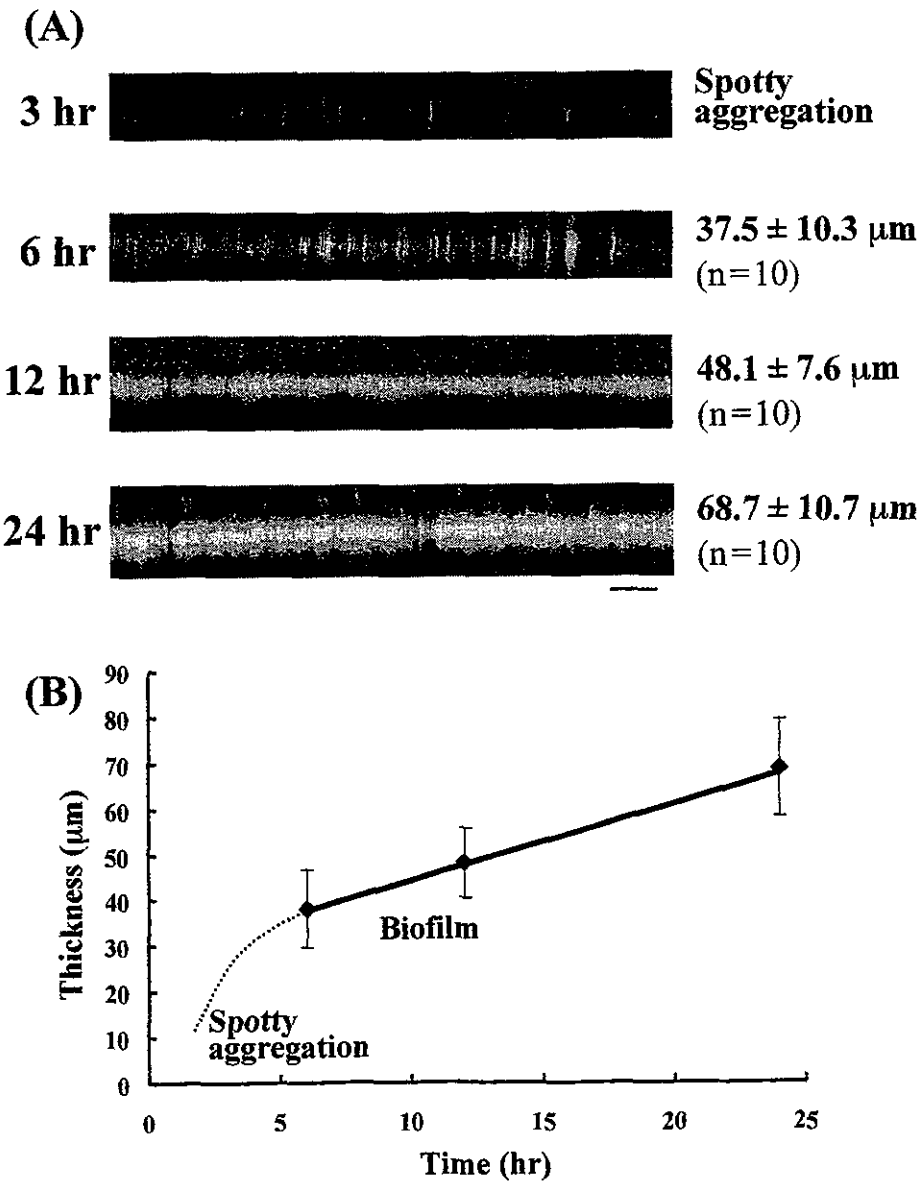

Figure 2. (A) CLSM photographs of vertical section of biofilms on PU at 3, 6, 12, and 24 h of incubations. Bar: 100 μm. (B) Biofilm thickness was determined by measuring the present images at 3, 6, 12, and 24 h of incubations. Ten vertical lines were randomly chosen for the analysis of each image. Values are expressed as means ± SD.

Protein coating of materials

Round PU sheets were incubated with bovine fibronectin (Itoham Foods Inc., Hyogo, Japan), bovine vitronectin (Yagai Co., Yamagata, Japan), and bovine serum albumin (Itoham Foods) at 1 mg/mL (0.1%) at 37°C for 24 h. Then, Luria-Bertani medium containing *E. coli* (2×10^5 CFU/mL) was poured over the protein-precoated round PU sheets and adherence was examined.

Statistical analysis

Statistical analysis was performed with the StatView 5.0 program (Abacus, Berkeley, CA). Data are shown as means ± SD. Statistical analysis was performed by analysis of variance. Differences at $p < 0.05$ were considered significant.

RESULTS

CLSM observation

To observe the 3D structure of the biofilm formed on the PU film, GFP-expressing YMel was cultured on the substrate under static condition for up to 24 h. After gentle washing with PBS, EPS generated during

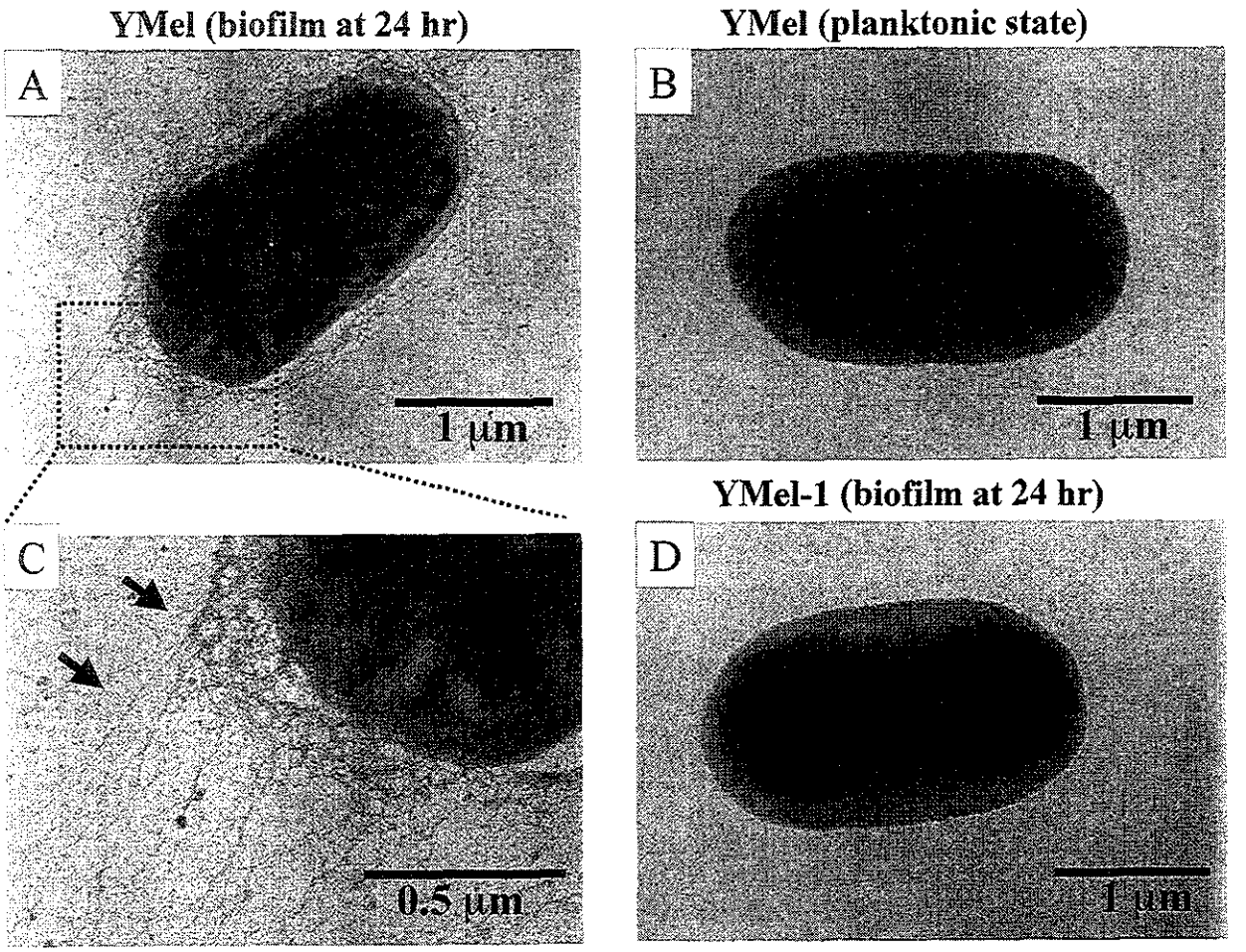

Figure 4. Transmission electron microscopic photographs by negative staining. (A) YMel in biofilm at 24 h; (B) YMel in planktonic state; (C) YMel in biofilm at 24 h with high magnification; and (D) YMel-1 in biofilm at 24 h. Arrows demonstrate curli.

orescence intensity remained almost constant, irrespective of the initial cell concentration.

Precoated-protein-dependent bacterial adhesion

To evaluate the effect of precoated proteins on bacterial adhesion, YMel was examined on round PU sheets precoated with the following proteins: fibronectin, vitronectin, and albumin (note that fibronectin and vitronectin are cell-adhesive, and albumin is non–cell-adhesive). As shown in Figure 7, for up to 12 h of incubation, there was a small significant difference in the number of adherent cells, irrespective of the type of precoated protein. However, at 24 h of incubation, the difference in the number of adherent cells was noted. The highest cell proliferation was observed on the fibronectin-coated surface, followed by the vitronectin-coated one, the proliferation potential of which was slightly higher than the noncoated surface; how-

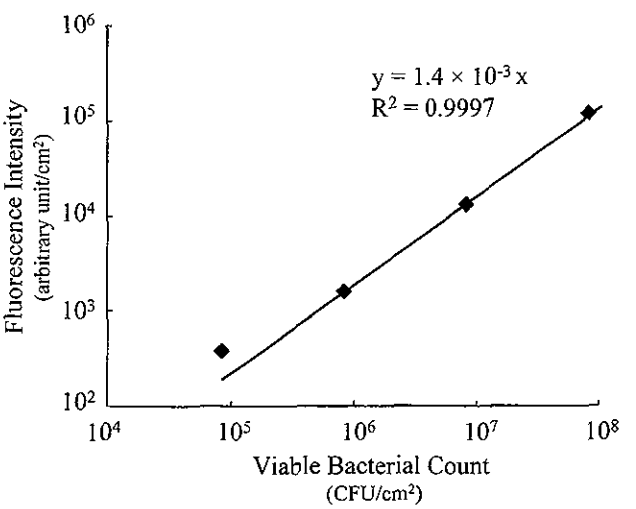

Figure 5. Correlation between fluorescence intensity and viable bacterial count in bacterial adhesion study at 24 h of incubation. The solution containing *E. coli* detached from PU sheets was diluted to different concentrations. Values are expressed as means ± SD.

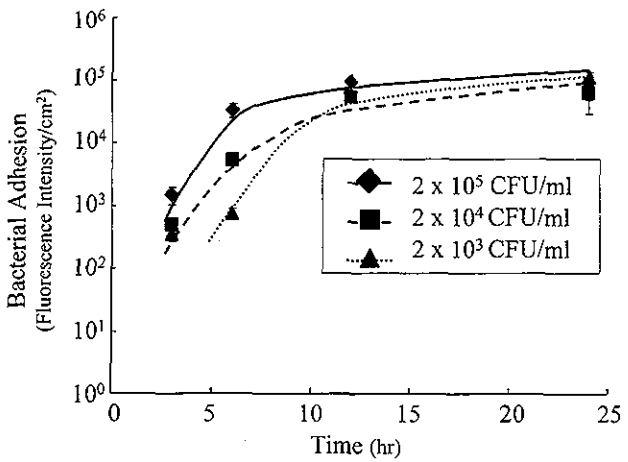

Figure 6. Time-dependent adhesion and proliferation of *E. coli* on PU. Initial concentration of bacterial cells: 2×10^3 (▲), 2×10^4 (■), 2×10^5, (◆) CFU/mL (n = 5). Values are expressed as means ± SD.

ever, there is only a small statistical difference between them. For the albumin-coated surface, although its initial adhesion potential is almost the same as that of the adhesive-protein-coated surfaces, minimal proliferation occured even with prolonged incubation time.

The curli-deficient mutant strain YMel-1 was used to determine the role of curli in bacterial adhesion. The curli-producing strain, YMel, and the curli-deficient isogenic mutant strain, YMel-1, were examined on PU surfaces with or without fibronectin coating. The number of adherent cells, measured by the plate count method, shows that the adhesion of YMel-1 was less than that of YMel to both fibronectin-coated and noncoated substrates. Precoating the PU sheets with fibronectin did not increase the adhesion of YMel-1 (Fig. 8), indicating that curli participate in fibronectin-mediated bacterial adhesion.

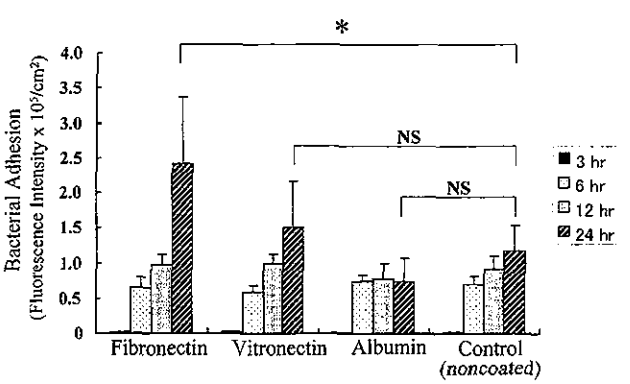

Figure 7. Bacterial adhesion to and proliferation on PU precoated with proteins at 3, 6, 12, and 24 h of incubations (n = 5). Control is noncoated PU. Values are expressed as means ± SD.

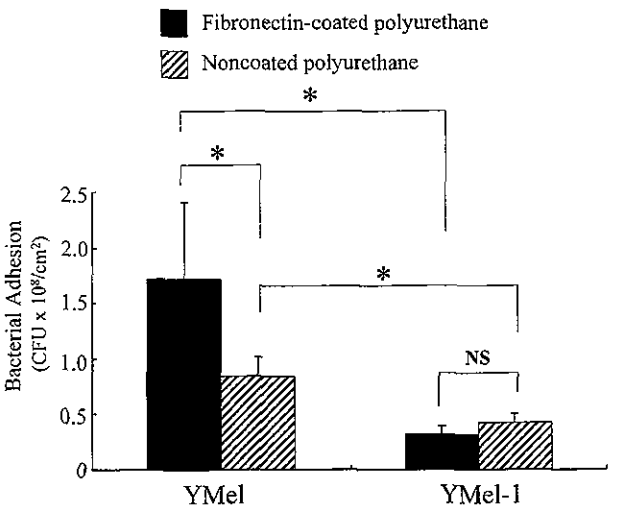

Figure 8. Bacterial adhesion and proliferation of curli-producing strain, YMel, and curli-deficient isogenic mutant strain, YMel-1 in fibronectin-coated PU and noncoated PU at 24 h of incubation (n = 5). Adhesion was determined by the plate count method. Values are expressed as means ± SD.

DISCUSSION

Bacterial adhesion is an important initial step in infection at the site of implanted biomaterials, which often causes life-threatening events in clinical situations.[1,2] Among bacteria capable of foreign-body-induced infection, *E. coli* is an important pathogen in the blockade of biliary stents or urinary catheters. The understanding of biofilm formation on synthetic biomaterials and the quantitative detection method for biofilm are key issues leading to the surface design of biomaterials with a high antibacterial adhesion potential. Electron microscopy has been used to examine biofilms on various materials.[9] However, sample preparation for electron microscopic observation requires sample dehydration, during which biofilms are often easily collapsed, structurally damaged, or destroyed. These dehydrated samples provide a deceivingly simplistic view of biofilms.[10]

To overcome this problem, we utilized fluorescent-compound-labeled *E. coli* strains that were transformed with a plasmid harboring the gene encoding GFP from jellyfish *Aequorea victoria* as an *in situ* cell marker. EPS are mainly responsible for the morphology and function of biofilms, and are considered to be key components that determine the physicochemical and biological properties of biofilms.[10,18] The co-use of GFP for bacteria and a fluorescent-compound-labeled marker specific to EPS in CLSM study provides new insights into the structure and nature of biofilm formation.

In our study, the imaging of 3D fine structures was acquired using fully hydrated samples for CLSM without any complex fixation such as the dehydration

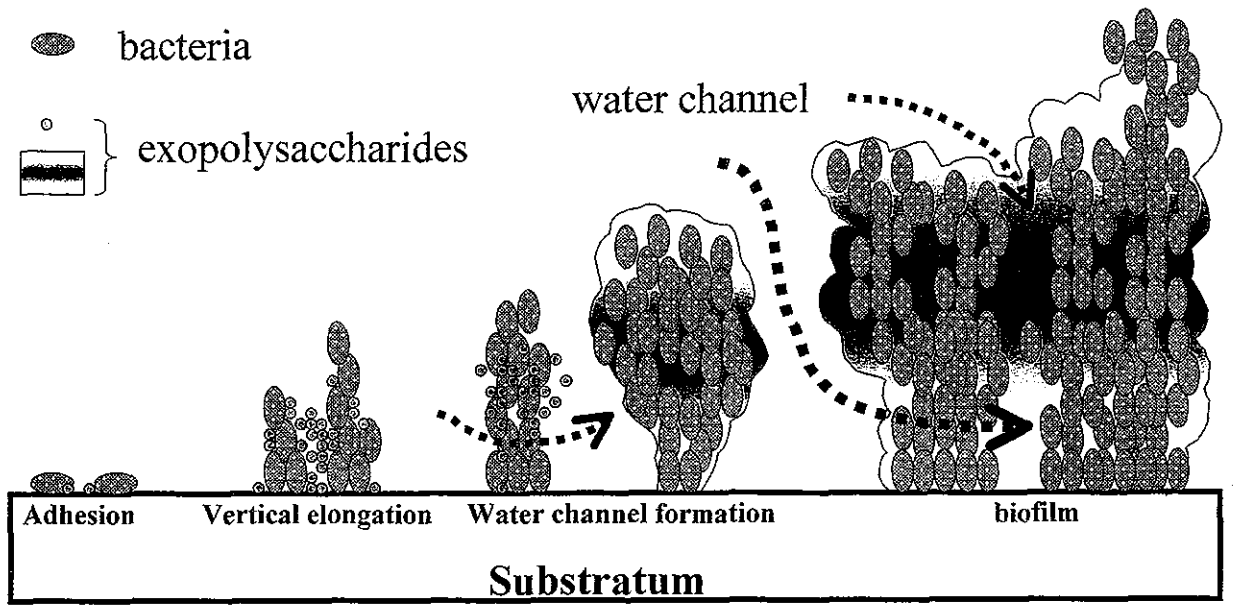

Figure 9. Scheme of time-dependent formation of biofilm architecture.

necessary in electron microscopy. In the early phase [3 h after plating: Figs. 1 and 2(A)], *E. coli* YMel emitting green fluorescence spottily aggregated on the PU surface and then vertically elongated. The number of aggregates increased with incubation time and scattered EPS-rich domains were observed [Figs. 1 and 2(A)]. Finally, a 3D structure including water channels was formed. The thickness of the biofilm increased with time, reaching to several tens of microns at 24 h after plating [Fig. 2(B)]. The channels as integral parts of the biofilm structure, which were identified as a black spotty area at 12 and 24 h of incubations (Fig. 1), are, in essence, the lifeline of the system, because they provide a means of circulating nutrients as well as exchanging metabolic products such as oxygen.[10] Interestingly, a dense interpenetrable structure of biofilm composed of *E. coli* and EPS, which was observed as the yellow region in Figures 1 and 2, existed at the middle part of the thick biofilm. Such time-dependent morphological events including bacterial adhesion, the secretion and organization of EPS, colony formation, and biofilm formation with water channels are shown in Figure 9.

As for the quantification of *E. coli* cells in biofilms, the fluorescence intensity of GFP expressed by adhered *E. coli* cells, which is directly proportional to the viable-bacterial count obtained by the plate count method (Fig. 5), allows us to easily and rapidly determine the number of adhered *E. coli* cells as compared with the conventional plate count method which requires overnight culture to detect colony formation. The growth rate of the *E. coli* cells examined for up to 24 h showed that the number of adhered and proliferated *E. coli* cells increased exponentially with time up to 12 h, and then appeared to increase at a markedly reduced rate with prolonged time, regardless of the initial bacterial cell concentration.

Many studies have reported that bacterial adhesion to and biofilm formation on material surfaces are affected by the type of protein adsorbed to the surfaces.[19-22] In the present study, three kinds of protein were preadsorbed: fibronectin and vitronectin as cell-adhesive proteins, and albumin as a non-cell-adhesive protein. Regardless of the presence or absence and the type of preadsorbed protein, there was only a small difference in the number of bacterial adhesion up to 12 h. Among the proteins tested, only fibronectin exhibited a markedly high proliferation activity only at 24 h of incubation, whereas albumin exhibited a high inhibitory activity against bacterial proliferation at 24 h of incubation. There is a small difference in bacterial proliferation activity between the vitronectin-coated and noncoated PU surfaces. This may be because the *E. coli* YMel does not produce curli in the early phase for up to 12 h of incubation but produces abundant curli (Fig. 4) in the biofilm at 24 h of incubation, although YMel does not produce curli in the planktonic state at 37°C.[23] These results are consistent with the finding by Kikuchi et al:[24] that curli were expressed in biofilm after growth at 37°C. Because curli specifically bind to fibronectin and are associated with biofilm maturation, curli-mediated biofilm formation occurred on the fibronectin-coated PU surface with a prolonged incubation time. However, the curli-deficient isogenic mutant, YMel-1, did not enhance bacterial adhesion and proliferation on the fibronectin-coated PU surface (Fig. 8).

In conclusion, we developed a novel method of deter-

mining morphological events during biofilm formation on synthetic polymers using GFP-expressing *E. coli* under CLSM observation, without the destruction of very fragile 3D structures, which may help logical surface design with a high antibacterial potential.

The authors thank T. Kikuchi, K. Yasutake, E. Koga, and M. Sato for technical assistance, and T. Kanemaru and A. Takade for electron microscopic examination.

References

1. An YH, Friedman RJ. Concise review of mechanisms of bacterial adhesion to biomaterial surfaces. J Biomed Mater Res 1998;43:338–348.
2. Gristina AG. Biomaterial-centered infection: microbial adhesion versus tissue integration. Science 1987;237:1588–1595.
3. Davies D. Understanding biofilm resistance to antibacterial agents. Nat Rev Drug Discov 2003;2:114–122.
4. Sung JY, Leung JW, Shaffer EA, Lam K, Costerton JW. Bacterial biofilm, brown pigment stone and blockage of biliary stents. J Gastroenterol Hepatol 1993;8:28–34.
5. Bryers JD, Hendricks S. Bacterial infection of biomaterials. Ann NY Acad Sci 1997;31:127–137.
6. Higashi JM, Wang IW, Shlaes DM, Anderson JM, Marchant RE. Adhesion of *Staphylococcus epidermidis* and transposon mutant strains to hydrophobic polyethylene. J Biomed Mater Res 1998; 39:341–350.
7. Merritt K, Gaind A, Anderson JM. Detection of bacterial adherence on biomedical polymers. J Biomed Mater Res 1998;39: 415–422.
8. Speer AG, Cotton PB, Rode J, Seddon AM, Neal CR, Holton J, Costerton JW. Biliary stent blockage with bacterial biofilm. A *light and electron microscopy study*. Ann Intern Med 1988;108: 546–553.
9. van Berkel AM, van Marle J, van Veen H, Groen AK, Huibregtse K. A scanning electron microscopic study of biliary stent materials. Gastrointest Endosc 2000;51:19–22.
10. Davey ME, O'toole GA. Microbial biofilms: from ecology to molecular genetics. Microbiol Mol Biol Rev 2000;64:847–867.
11. Cowan SE, Gilbert E, Khlebnikov A, Keasling JD. Dual labeling with green fluorescent proteins for confocal microscopy. Appl Environ Microbiol 2000;66:413–418.
12. Decho AW, Kawaguchi T. Confocal imaging of *in situ* natural microbial communities and their extracellular polymeric secretions using Nanoplast resin. Biotechniques 1999; 27:1246–1252.
13. Strathmann M, Wingender J, Flemming HC. Application of fluorescently labelled lectins for the visualization and biochemical characterization of polysaccharides in biofilms of *Pseudomonas aeruginosa*. J Microbiol Methods 2002;50:237–248.
14. Olsen A, Wick MJ, Morgelin M, Bjorck L. Curli, fibrous surface *proteins of Escherichia coli*, interact with major histocompatibility complex class I molecules. Infect Immun 1998;66:944–949.
15. Prigent Combaret C, Prensier G, Le Thi TT, Vidal O, Lejeune P, Dorel C. Developmental pathway for biofilm formation in curli-producing *Escherichia coli* strains: role of flagella, curli and colanic acid. Environ Microbiol 2000;2:450–464.
16. Olsen A, Jonsson A, Normark S. Fibronectin binding mediated by a novel class of surface organelles on *Escherichia coli*. Nature 1989;338:652–655.
17. Andersen JB, Sternberg C, Poulsen LK, Bjorn SP, Givskov M, Molin S. New unstable variants of green fluorescent protein for studies of transient gene expression in bacteria. Appl Environ Microbiol 1998;64:2240–2246.
18. Danese PN, Pratt LA, Kolter R. Exopolysaccharide production is required for development of *Escherichia coli* K-12 biofilm architecture. J Bacteriol 2000;182:3593–3596.
19. Froman G, Switalski LM, Faris A, Wadstrom T, Hook M. Binding of *Escherichia coli* to fibronectin. A mechanism of tissue adherence. J Biol Chem 1984;259:14899–14905.
20. Yu JL, Ljungh A, Andersson R, Jakab E, Bengmark S, Wadstrom T. Promotion of *Escherichia coli* adherence to rubber slices by adsorbed fibronectin. J Med Microbiol 1994;41:133–138.
21. Yu JL, Andersson R, Wang LQ, Bengmark S, Ljungh A. Fibronectin on the surface of biliary drain materials: a role in bacterial adherence. J Surg Res 1995;59:596–600.
22. Yu JL, Andersson R, Ljungh A. Protein adsorption and bacterial adhesion to biliary stent materials. J Surg Res 1996;62:69–73.
23. Bian Z, Brauner A, Li Y, Normark S. Expression of and cytokine activation by *Escherichia coli* curli fibers in human sepsis. J Infect Dis 2000;181:602–612.
24. Kikuchi T, Mizunoe Y, Takade A, Yoshida S. Curli is required for development of biofilm architecture in *Escherichia coli* K-12 *and enhance bacterial adherence to human uroepithelial cells*. In preparation.

nature neuroscience

Developmental switch from GABA to glycine release in single central synaptic terminals

Junichi Nabekura[1,2,5] Shutaro Katsurabayashi[1,5], Yasuhiro Kakazu[1], Shumei Shibata[1], Atsushi Matsubara[3], Shozo Jinno[4], Yoshito Mizoguchi[1], Akira Sasaki[3] & Hitoshi Ishibashi[1]

Early in postnatal development, inhibitory inputs to rat lateral superior olive (LSO) neurons change from releasing predominantly GABA to releasing predominantly glycine into the synapse. Here we show that spontaneous miniature inhibitory postsynaptic currents (mIPSCs) also change from GABAergic to glycinergic over the first two postnatal weeks. Many 'mixed' mIPSCs, resulting from co-release of glycine and GABA from the same vesicles, are seen during this transition. Immunohistochemistry showed that a large number of terminals contained both GABA and glycine at postnatal day 8 (P8). By P14, both the content of GABA in these mixed terminals and the contribution of GABA to the mixed mIPSCs had decreased. The content of glycine in terminals increased over the same period. Our results indicate that switching from GABAergic to glycinergic inputs to the LSO may occur at the level of a single presynaptic terminal. This demonstrates a new form of developmental plasticity at the level of a single central synapse.

GABA and glycine are the major inhibitory transmitters in the mammalian central nervous system. Although they act at separate receptors, they can be co-released from single synaptic terminals projecting onto spinal motor neurons and brainstem trigeminal neurons[1,2]. Postsynaptic clusters of both glycine and $GABA_A$ receptors appear to be co-localized at the subsynaptic membrane[3,4]. Furthermore, mIPSCs recorded from spinal neurons include both GABAergic and glycinergic components, suggesting that both GABA and glycine are co-released from a single synaptic vesicle[5,6]. Hence, at spinal cord synapses, GABA and glycinergic transmission is closely related, and this could have important implications for the strength and timing of motor neuron inhibition[7].

The coordinated combination of GABAergic and glycinergic inhibitory transmission is also functionally critical in the lateral and medial superior olive auditory relay neurons (LSO and MSO neurons, respectively)[8,9]. In the normal development of the auditory system, inhibitory synaptic transmission in the LSO and MSO changes from being predominantly GABAergic to being predominantly glycinergic[8,9]. Structural reorganization of the inhibitory synapses between the medial nucleus of the trapezoidal body (MNTB) and the LSO also occur throughout development[10], and it is unclear whether this switch from GABA to glycine occurs via a selective loss of GABAergic synapses and an increase in glycinergic synapses, or whether this transmitter switch occurs at individual synapses. Developmental changes in receptor subunit expression patterns have been observed in the LSO[11], but there have been no reports of a presynaptic change in the nature of the released neurotransmitter at the level of a single synapse. In the present study, we further elucidate the mechanisms contributing to this neurotransmitter switch, particularly focusing on whether presynaptic changes occur and whether they occur at single synapses.

RESULTS

Evoked IPSCs (eIPSCs) were recorded from LSO neurons in response to electrical stimulation of the ventromedial part of the LSO slice preparation. Both CNQX (10^{-5} M) and APV (10^{-5} M) were added to the external solution to block glutamatergic responses. In LSO neurons from P2 rats, bicuculline (10^{-5} M) inhibited the eIPSC by about 70%, but only caused a mild (about 15%) inhibition in P14 rats (Fig. 1a,b). The bicuculline-insensitive component of the eIPSC was completely abolished, at all ages, by adding strychnine (10^{-6} M). The inhibitory effects of bicuculline on muscimol and glycine responses were stable in potency throughout development (Fig. 1c). Thus, inhibitory synaptic transmission to LSO neurons changed from predominantly GABAergic to predominantly glycinergic during development. The switch is evident by P7, which is somewhat earlier than observed in the gerbil LSO[8], although it is virtually completed by this time for inhibitory inputs to the rat MSO[9].

To elucidate the underlying cause of this switch from predominantly GABAergic to predominantly glycinergic inputs, we concentrated on the nature of miniature IPSCs (mIPSCs), which are considered to be single quantal events[12,13]. We mechanically dissociated LSO neurons with adherent presynaptic terminals[14] (Fig. 2a) and recorded mIPSCs at a V_H of –60 mV in the presence of CNQX (10^{-5} M), APV (10^{-5} M) and tetrodotoxin (TTX; 3×10^{-7} M). This preparation allows us to measure spontaneous synaptic currents under good space-clamp conditions and without complications from other neurons or glia[14]. We

[1]Department of Cellular and System Physiology, Graduate School of Medical Sciences, Kyushu University, Fukuoka 812-8582, Japan. [2]Department of Developmental Physiology, National Institute for Physiological Sciences, Okazaki 444-8585, Japan. [3]Department of Otorhinolaryngology, School of Medicine, Hirosaki University, Hirosaki 036-8562, Japan. [4]Department of Anatomy and Neurobiology, Graduate School of Medical Sciences, Kyushu University, Fukuoka 812-8582, Japan. [5]These authors contributed equally to this work. Correspondence should be addressed to J.N. (nabekura@nips.ac.jp).

Published online 21 December 2003; doi:10.1038/nn1170

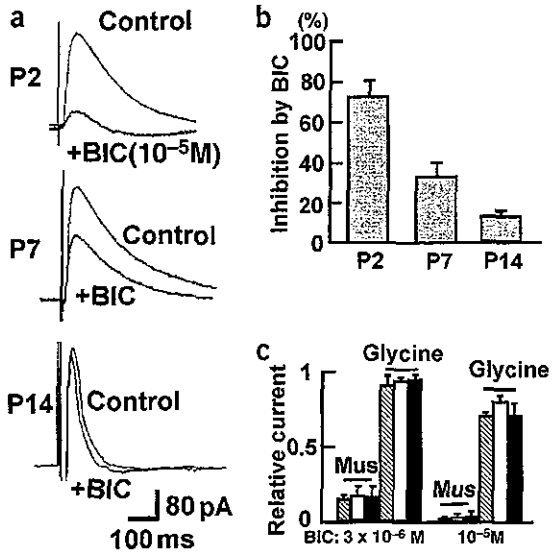

Figure 1 Developmental change in the bicuculline sensitivity of IPSCs recorded in LSO neurons in response to electrical stimulation of the ventromedial aspect of the LSO brain slice. (**a**) Five representative averaged evoked IPSCs, recorded from P2, P7 and P14 rats, in the absence (Control) and presence of 10^{-5} M bicuculline (+BIC). We used bicuculline rather than strychnine to discriminate between $GABA_A$ and glycine receptor responses because the potency of strychnine on muscimol (which affect $GABA_A$ receptors) responses varied during development (unpublished data). (**b**) Mean data showing the relative inhibition of eIPSCs by bicuculline, in LSO neurons from different developmental stages ($n = 6$, respectively). Evoked IPSCs were recorded using standard whole-cell patch-clamp techniques. V_H was 0 mV. (**c**) Inhibition of 10^{-5} M muscimol and 3×10^{-5} M glycine evoked responses by 3×10^{-6} and 10^{-5} M bicuculline, in LSO neurons from P0–2 (strip columns), P6–8 (open columns) and P14–16 (closed columns) rats. Response amplitudes are plotted relative to that observed in the absence of bicuculline ($n = 5$ or 6 in each case). The relative inhibitory effect of bicuculline on $GABA_A$ and glycine receptor mediated responses was constant throughout development.

initially pharmacologically isolated GABAergic and glycinergic components of mIPSCs in LSO neurons from P6–7 rats (Fig. 2b, left). In the presence of bicuculline (5×10^{-6} M), glycinergic mIPSCs were observed with a relatively fast decay time constant (fit from 90–10% of the mIPSC amplitude, $\tau_{gly} = 7.2 \pm 1.3$ ms, mean ± s.e.m., $n = 5$ neurons, Fig. 2c,d). In the same neurons, GABAergic mIPSCs, in the presence of strychnine (3×10^{-7} M), were observed with a much slower decay time constant ($\tau_{GABA} = 73.6 \pm 4.5$ ms, $n = 5$, Fig. 2c,d). In three other neurons, the mIPSC decay in the presence of another selective $GABA_A$ antagonist, SR-95531, was fit with a similar time constant as observed in the presence of bicuculline ($\tau_{gly} = 8.3 \pm 2.2$ ms). These results are consistent with previous reports that GABAergic mIPSCs are characterized by a longer current decay time than are glycinergic mIPSCs[6,15,16] and indicate that the mIPSCs contain both $GABA_A$ receptor– and glycine receptor–mediated components. Indeed, in control conditions, mIPSCs with two components were also detected (Fig. 2b, right). The decay of these dual-component, 'mixed' mIPSCs was fit with the sum of two exponentials, a τ_{fast} and τ_{slow}, which were 6.2 ± 0.9 ms and 58.7 ± 10.3 ms, respectively ($n = 5$; Fig. 2d). These time constants were very similar to the pharmacologically isolated τ_{gly} and τ_{GABA}, and this excellent agreement between τ_{slow} and τ_{GABA}, and between τ_{fast} and τ_{gly} was found throughout development. In neurons from P1–2 rats, τ_{fast} was 7.3 ± 3.4 ms ($n = 5$) and τ_{gly} was 8.3 ± 2.5 ms ($n = 5$), whereas τ_{slow} was 84.2 ± 8.5 ms ($n = 5$) and τ_{GABA} was 92.9 ± 10.2 ms ($n = 5$). In neurons from older rats (P16–17), τ_{fast} was 3.4 ± 1.4 ms ($n = 5$) and τ_{gly} was 3.7 ± 1.5 ms ($n = 5$), whereas τ_{slow} was 42.2 ± 6.4 ms ($n = 5$) and τ_{GABA} was 38.2 ± 7.2 ms ($n = 5$). These results show that these mixed mIPSCs reflect co-release of GABA and glycine from a single vesicle. They also show how the mIPSC decay constants get faster during development, presumably reflecting changes in receptor subunit composition[17].

Just as was observed for the eIPSCs, the chemical nature of mIPSCs also changed from predominantly GABAergic to predominantly glycinergic (Fig. 3). In the absence of any strychnine or

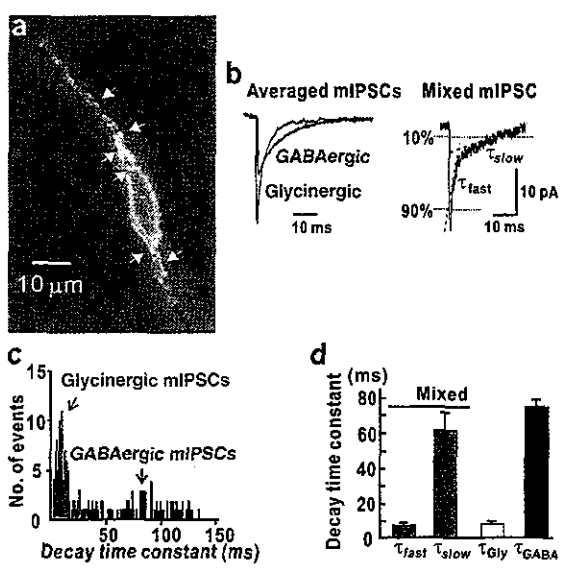

Figure 2 Pharmacological and kinetic isolation of GABAergic, glycinergic and mixed mIPSCs in voltage-clamped, isolated LSO neurons. (**a**) *Photograph of a mechanically dissociated LSO neuron from P7 rats* showing adherent functional synaptic boutons stained green with FM1-43. FM1-43 (1 mM) was added to the perfusate with 20 mM K^+ for 3 min, then washed out with Ca^{2+}-free, standard extracellular solution. Arrowheads *indicate examples of stained synaptic boutons.* (**b**) Left, averaged mIPSCs recorded in the presence of strychnine (300 nM, GABAergic mIPSC, blue, $n = 121$) and in the presence of bicuculline (5 µM, glycinergic mIPSC, red, $n = 96$) from a LSO neuron isolated from a P7 rat. Right, a 'mixed' mIPSC with a decay composed of both fast and slow components, recorded in the absence of any receptor antagonists in a LSO neuron from a P7 rat. (**c**) Distribution of the decay time constants of GABAergic (blue bars, strychnine 300 nM) and glycinergic mIPSCs (red bars, bicuculline, 5 µM) in an LSO neuron from P7 rat. Bin size, 1 ms. (**d**) Mean decay time constants for the three types of mIPSCs (mean ± s.e.m., $n = 5$ in each case). The mixed mIPSCs were fit by the sum of two exponential equations with time constants τ_{fast} and τ_{slow}, that corresponded to the decay time constants of the pharmacologically isolated glycinergic (τ_{gly}) and GABAergic (τ_{GABA}) mIPSCs, respectively.

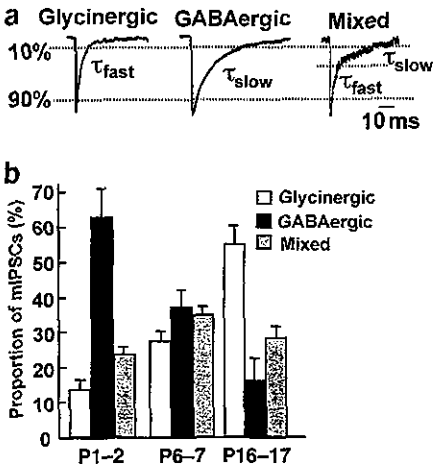

Figure 3 Developmental change in mIPSCs recorded in isolated LSO neurons. (**a**) Typical examples of GABAergic, glycinergic and mixed mIPSCs in a P6 LSO neuron. Horizontal bars indicate how the mIPSC decay, from 90% to 10% of the peak amplitude, was fit with one or two exponential functions (see **Fig. 2b**). The traces were obtained from a P6 LSO neuron. (**b**) Relative proportion of GABAergic (closed columns), glycinergic (open columns) and mixed mIPSCs (gray columns) in LSO neurons from P1–2, P6–7 and P16–17 rats. The proportion of mIPSCs of each type are expressed relative to the total number of mIPSCs recorded in each neuron (>200 events in each neuron), and are the mean ± s.e.m. of results from 10–12 neurons in each age group.

bicuculline, individual mIPSCs which were fit to either τ_{fast} or τ_{slow} were defined as glycinergic and GABAergic events, respectively (Fig. 3a). In P1–2 neurons, the proportion of total mIPSCs whose decay times indicated that they were GABAergic was 63.0 ± 7.5%, and in neurons from P16–17 the proportion was 16.0 ± 6.5%. At the same ages the proportions of glycinergic mIPSCs were 13.6 ± 2.8% and 55.3 ± 5.2%, respectively (Fig. 3b). The remainder of the mIPSCs had dual-component decay times (mixed mIPSCs). The incidence of these mixed mIPSCs was highest at P6–7 where they comprised 34.9 ± 2.5% of all mIPSCs ($n = 10$). In P1–2 and P16–17 rats, mixed mIPSCs comprised 23.4 ± 2.3% ($n = 10$) and 28.6 ± 3.2% ($n = 12$), respectively, of the total mIPSCs.

The mixed mIPSCs result from co-release of GABA and glycine from a single vesicle. To address whether the response to single vesicles shows a developmental change from GABAergic to glycinergic, we analyzed the relative contribution of the GABAergic (y_{GABA}) and glycinergic (y_{gly}) components to the total peak amplitude (y) of the mixed mIPSCs (Fig. 4a). If neurotransmitter switching also occurs at the level of single synapses, the GABAergic component in the mixed mIPSCs would be expected to decrease with age and the glycinergic component would increase. The absolute amplitude of the glycinergic component increased with age: 15.6 ± 3.2 pA at P1–2, 27.9 ± 3.6 pA at P6–7 and 43.4 ± 8.2 pA at P16–17 (n = 10–12 neurons at each age). The amplitude of the GABAergic component also increased from P1–2 (10.5 ± 2.9 pA, $n = 10$) to P6–7 (19.0 ± 1.5 pA, $n = 10$), before declining again in older rats (13.3 ± 1.7 pA at P16–17, $n = 12$, Fig. 4c). The relative contribution of the GABAergic component to the total mixed mIPSC amplitude (y_{GABA}/y) was not significantly different between P1–2 and P6–7 rats, but was decreased in older (P16–17) rats (38.9 ± 3.5% at P1–2, 53.2 ± 5.9% at P6–7 and 25.8 ± 3.9% at P16–17, Fig. 4b,d). Thus, the contribution of GABA to the response to a single vesicle declines in older rats, whereas that of glycine increases, consistent with neurotransmitter switching occurring at a single synapse.

The above results demonstrate a developmental switch from GABAergic to glycinergic neurotransmission at single synapses but do not distinguish whether this change occurs presynaptically (that is, a single terminal switches from GABA to glycine release), or postsynaptically (that is, a change in subsynaptic receptors from $GABA_A$ to glycine[8,11] with a constant co-release of GABA and glycine throughout development[16]), or a combination of both. The mean responses of LSO neurons to exogenous GABA and glycine were not significantly different throughout development. Specifically, GABA (3×10^{-5} M) induced an inward current at a V_H of –60 mV of 305 ± 68 pA in neurons from P0–2 rats, 409 ± 38 pA from P7 rats and 364 ± 82 pA from P14 rats (n = 5 or 6 neurons at each age). At the same ages the response to glycine (10^{-4} M) was 297 ± 57 pA at P0–2, 349 ± 84 pA at P7 and 305 ± 58 pA at P14 (n = 5 or 6). Therefore, there does not seem to be any gross developmental change in the response of the extrasynaptic receptors, although this may not reflect what is occurring at the subsynaptic receptors.

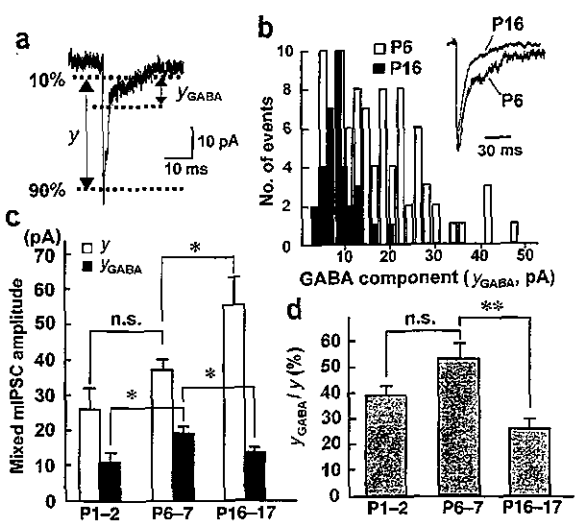

Figure 4 Developmental decrease in the contribution of the GABAergic component to mixed mIPCSs. (**a**) Example of a mixed mIPSC to illustrate the meaning of y (the peak mIPSC amplitude) and y_{GABA} (the amplitude of the mIPSC due to the GABAergic component). Individual events were fit with the double exponential function: $y = y_0 + y_{fast}\, e^{(-x/\tau fast)} + y_{slow}\, e^{(-x/\tau slow)}$, in which y_{fast} and y_{slow} were defined as $y_{glycine}$ and y_{GABA} and their sum as y. (**b**) Distribution of y_{GABA} in mixed mIPSCs from typical P6 (open bars) and P16 (black bars) LSO neurons. mIPSCs from P6 and P16 neurons were scaled so as to make their peak amplitudes equivalent. Note that the GABAergic component (y_{GABA}) of the mixed mIPSCs in P16 LSO neurons was smaller than that in P6 LSO neurons. Bin size, 2 pA. (**c**) Comparison of the mean absolute peak amplitude of mixed mIPSCs (y, open bars) and the mean amplitude of the GABAergic component (y_{GABA}, closed bars) in different age groups. Note the steady increase in y throughout development and the smaller contribution of y_{GABA} in the P16–17 rats. (**d**) Relative contribution of the GABAergic component to the peak amplitude of the mixed mIPSCs (y_{GABA}/y) at different developmental stages. Note the marked decrease in y_{GABA}/y after P6–7.

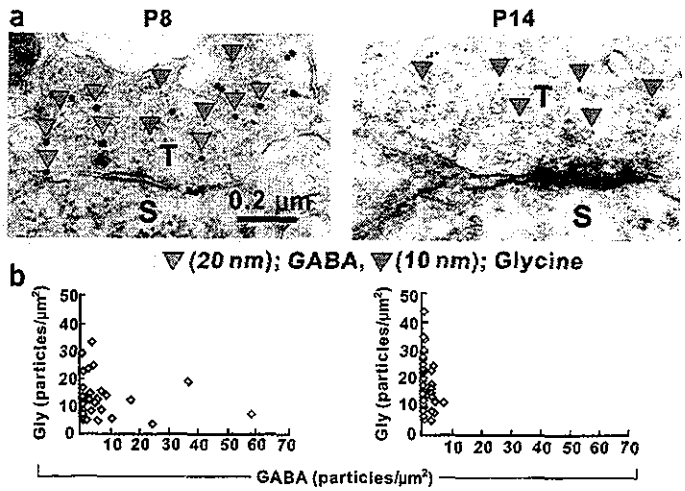

Figure 5 Quantitative analysis of GABA and glycine content in presynaptic terminals using immunogold staining and electron microscopy. (a) Typical electron micrographs of a synapse on to an LSO neuron; in a P8 (left) and P14 (right) rat. The large (20 nm) gold particles indicated with blue arrow heads are coated with antibodies specific to GABA, whereas the smaller (10 nm) gold particles are coated with antibodies to glycine (red arrowheads). T, presynaptic terminal; S, soma of postsynaptic cell. (b) Summary of group data from the immunogold experiments in P8 (left) and P14 (right) LSO neurons. Number of GABA-reactive particles/μm² in each inhibitory synapse is plotted against the number of glycine-reactive gold particles observed in the same synapse (total number of terminal micrographs observed were 58 from three P8 rats, and 80 from three P14 rats). Note that all inhibitory synapses observed contained glycine, but significant quantities of GABA were only colocalized in these synapses from the P8 neurons. The number of glycine particles was greater in P14 synapses than in P8 synapses ($P < 0.05$, unpaired t-test). The specificity of each antibody was examined using control experiments (**Supplementary Fig. 2**).

We also examined any presynaptic changes during development by looking directly at the composition of transmitters in single presynaptic terminals using an immunogold technique and electron microscopy (Fig. 5). Many terminals showed a background stain of about 1–5 gold particles/μm², so only terminals with a total number of GABA- and glycine-reactive particles greater than this background level were considered to be clearly inhibitory synapses and included in the subsequent analysis (**Supplementary Fig. 1 online**). At P8, 38/58 terminals satisfied this criterion, and at P14, 41/80 terminals were included. At P14, the density of glycine-reactive gold particles in a single terminal was 18.6 ± 1.5/μm² (mean ± s.e.m., $n = 41$), which was significantly larger than observed at P8 (11.8 ± 1.2 particles/μm², $n = 38$, $P < 0.05$, unpaired t-test, Fig. 5b). In contrast, the GABA particle density in single terminals significantly decreased over the same period, from 4.9 ± 1.8/μm² at P8 ($n = 38$) to 0.9 ± 0.30/μm² at P14 ($n = 41$; $P < 0.05$). The percentage of terminals where both GABA- and glycine-reactive gold particles were observed, decreased from 50% at P8 (19/38 terminals) to 32% (13/41) at P14. Hence, switching of inhibition from GABAergic to glycinergic is also reflected in an increase in glycine content in terminals, a decrease in the proportion of terminals containing GABA, and a decrease in the extent of GABA in terminals where both transmitters are present.

One mechanism that potentially could decrease the amount of GABA in single presynaptic terminals is a decrease in the synthesis of GABA in the LSO. To investigate this possibility, we used immunohisto-chemistry and confocal microscopy to examine levels of the GABA synthesizing enzyme, glutamic acid decarboxylase (GAD). For comparison, we also stained for glycine in these experiments. The glycine antibody staining in the LSO markedly increaseed in intensity during development, whereas GAD antibody staining (which recognizes both GAD 65 and GAD 67) seemed to decrease in intensity over the same period (Fig. 6). At higher resolution (Fig. 6g–l), similar changes in the number of GAD- and glycine-reactive puncta are seen, although several terminals still showed clear GAD staining even at P18 (Fig. 6k). This developmental pattern of glycine staining parallels that observed in the immunogold experiments (Fig. 5). The decrease in GAD staining suggests that a decrease in GABA synthesis contributes to the decrease in the GABA content in individual terminals.

Finally, we examined whether the extent of occupation of the postsynaptic GABA receptor clusters changes during the transitional period when the contribution of GABA to mIPSCs is changing. In three out of seven neurons from P6 rats, diazepam (3×10^{-7} M) increased the mean amplitude of mIPSCs by about 6–16%. This suggests that, for these three neurons, the GABA content in a single vesicle does not saturate the subsynaptic $GABA_A$ receptors. Given that the concentration of GABA in the synaptic cleft at individual release sites is typically sufficient to saturate postsynaptic $GABA_A$ receptor clusters in central neurons[18], this result further supports the decreased content of GABA in single vesicles and suggests that the presynaptic decreases in GABA may occur before significant decreases in the number of postsynaptic receptors[11].

DISCUSSION

In the present study, we used both electrophysiological analysis of mIPSCs and immunohistochemistry to show that the neurotransmitter phenotype of single presynaptic inhibitory terminals changes from GABAergic to glycinergic during the first two postnatal weeks. An initial period of expansion of both MNTB terminal arborizations and LSO dendrites in the first one or two postnatal weeks is followed by a refinement of these processes and a loss of synaptic specializations[19]. Recent studies indicate that the functional elimination of inhibitory inputs from MNTB to the LSO may occur before the structural changes, even within the first two weeks[20]. If synapse elimination and refinement were solely responsible for this presynaptic switch, terminals would need to be selectively eliminated based on subtle differences in their relative presynaptic GABA and glycine content, and sequentially replaced with glycinergic terminals containing an increasing amount of glycine and a decreasing amount of GABA. We strongly favor a much simpler hypothesis; that the concentration of glycine increases, while that of GABA decreases, in single terminals. This inference is also supported by the decrease in GAD levels (Fig. 6). Considering that the vesicular inhibitory amino acid transporter (VIAAT) can pump both GABA and glycine into the presynaptic vesicles[21], this developmental change in terminal GABA/glycine content is then reflected in the vesicular content of GABA/glycine and the

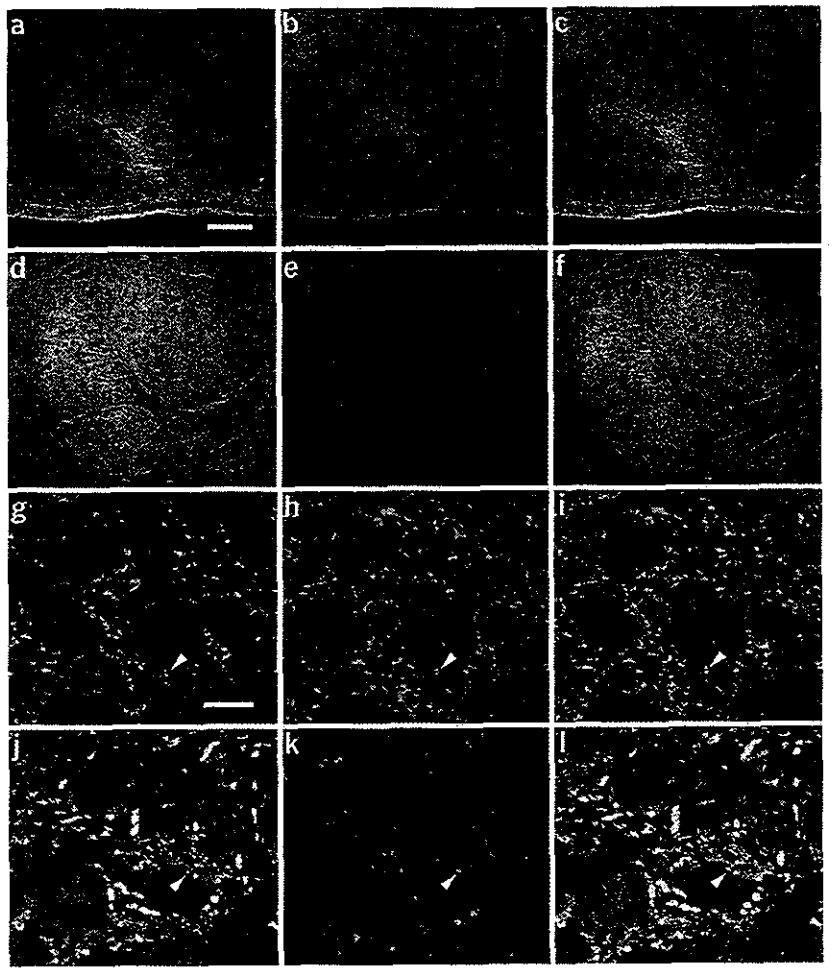

Figure 6 Immunohistochemical staining of GAD and glycine in the developing LSO. Immunofluorescent double-labeled confocal laser scanning microscope images for glycine (**a,d,g,j**), glutamic acid decarboxylase (GAD; **b,e,h,k**) and when both images are merged (**c,f,i,l**). Both lower-magnification images (**a–f**) and higher-power images (**g–l**) from sections from P5 (**a–c**, g–i) and P18 rats (**d–f**, j–l) are shown. At P5, there is weak glycine immunoreactivity throughout the LSO but intense GAD immunoreactivity (**a–c**). The high-power images (**g–i**) further show that only a few glycine-positive puncta exist in the LSO, whereas there are numerous GAD-positive puncta. At P18, the low-power images (**d–f**) show the intense glycine immunoreactivity and the weak GAD immunoreactivity in the LSO. The high-power images (**j–l**) reveal that many glycine-positive puncta are present in the LSO, but there are only a few GAD-positive puncta. Arrowheads indicate example boutons containing both glycine and GAD immunoreactivity. The scale bar in **a** applies to the low-power images (**a–f**; 100 μm); the scale bar in g applies to the high-power images (g–l; 10 μm). Under our experimental conditions, soma staining for GAD and glycine in the LSO neurons is not shown as clearly as that for the presynaptic boutons. Staining and image-capturing conditions were optimized for visualization of boutons.

decay time course of the mixed mIPSCs. Our preliminary data indicate that VIAAT is expressed at relatively high levels in the rat LSO. A change in the content of neurotransmitter, from noradrenaline to acetylcholine, has also been found in peripheral sympathetic nerve terminals following innervation of their targets in the sweat gland[22,23]. A switch from GABA to glycine has already been reported for IPSCs evoked by stimulation of multiple MNTB inputs[8–11], but here we provide new evidence that neurotransmitter switching at a central synapse can occur at the level of a single presynaptic vesicle.

One intriguing result from the present study is that although the switch from GABAergic to glycinergic eIPSCs was evident at P7 (Fig. 1) and there was a decline in the proportion of GABAergic mIPSCs over the same period, the contribution of GABA to the mixed mIPSCs did not significantly decrease until after the second postnatal week (Fig. 4). One possible explanation for this difference is that switching of terminal and vesicle neurotransmitter content may occur over a shorter time period in individual terminals, but these effects in a population of terminals may not be apparent until later. For example, pure GABAergic terminals may be converted to a mixed phenotype in the first postnatal week, while at the same time, other mixed terminals are converted to pure glycinergic terminals (and hence would no longer be included in the population of mixed mIPSCs). If such temporal heterogeneity does occur, one may not expect to see changes in the population responses until all the terminals had already showed significant switching.

Presynaptic changes in neurotransmitter content, that is, an increase in glycine and a decrease in GABA, can be added to the range of changes in inhibitory synaptic transmission and its modulation that have been reported in the LSO throughout development. Morphological changes include extensive remodeling of pre- and postsynaptic elements. In the first postnatal week, expansion of MNTB afferents is apparent in the gerbil LSO, and this is followed by a more prolonged period (for up to 4 weeks) of refinement and elimination of both the terminal boutons and the LSO dendrites[10,19]. For the rat LSO, the number of dendritic end-points begins to decline during the first postnatal week, although the most marked decreases in the relative size of LSO dendrites and their fields occurs after P14 (ref. 24). Synapse elimination and functional reorganization of MNTB–LSO connections have also been recently demonstrated in the rat[20]. In this previous study, the functional refinement of the inhibitory inputs was completed by P8, suggesting that functional refinement of the inhibitory inputs may precede structural refinements. The shift from GABAergic to glycinergic eIPSCs in the gerbil occurs slightly later than observed for rat LSO (Fig. 1) and MSO inputs[9]—it is only about 40% complete by P8 (ref. 8). If synapse elimination is in fact completed by P8 in the rat, this would further support our hypothesis of changes in transmitter content in preexisting synapses. Our demonstration of mixed mIPSCs also indicates that glycine and $GABA_A$ receptors are colocalized at LSO synapses. Changes in receptors and their associated accessory proteins have also been reported in the developing LSO. Gephyrin immunoreactivity is very low at birth in the gerbil LSO but increases markedly over the first few weeks[8]. Antibody staining for $GABA_A$ receptor subunits β2

and β3 shows a parallel decline over this period[8]. Expression of the glycine α1 receptor subunit increases markedly over the first 2 weeks[10], replacing the neonatal (presumed α2) receptor isoform. This subunit switch is likely to contribute to the briefer decay times of glycinergic mIPSCs over the course of development[25]. The increased amplitude of glycinergic mIPSCs could also reflect changes in subsynaptic receptors, although we did not observe any developmental change in the amplitude of responses to exogenous glycine.

What could be the functional significance of the switch from GABAergic to glycinergic transmission? Both GABA and glycine depolarize neonatal LSO neurons due to their high intracellular Cl^- content[26,27]. The depolarizing GABA/glycine responses in the rat LSO convert to hyperpolarizing responses during the first two postnatal weeks[26]. This occurs because, in more mature neurons, the outwardly directed Cl^- transporter, KCC-2, is integrated into the plasma membrane and becomes functional[28]. The longer-duration GABAergic responses observed in this study and others[9] would be expected to produce a more prolonged depolarization than glycine would produce, thereby allowing greater Ca^{2+} influx. In fact, Ca^{2+} transients in response to MNTB stimulation have been observed in rat and mice LSO neurons during the first postnatal week[29]. The Ca^{2+} transients generated by exogenous GABA were also larger than those generated by exogenous glycine (although the synaptic Ca^{2+} transients were similar for GABAergic and glycinergic inputs)[29]. GABA-induced membrane depolarization in immature neurons has been shown to be important for neuronal maturation[30–32]. The aggregation of glycine receptors by gephyrin, for example, is promoted by Ca^{2+} influx through channels in the postsynaptic membrane[33]. Thus, GABA-induced elevation of Ca^{2+} might be similarly important for insertion of glycine receptors into the subsynaptic membrane in developing LSO neurons.

Another possible contribution from the GABAergic inhibition in the younger rats concerns $GABA_B$ receptor–mediated responses. In LSO neurons from P4–P8 rats, postsynaptic $GABA_B$ receptors mediate a form of frequency-dependent synaptic plasticity[34,35]. Hence GABAergic neurotransmission may also be important in developing LSO neurons due to actions via $GABA_B$ receptors.

In the adult, the briefer hyperpolarizing responses mediated by glycine receptors would be more appropriate for accurate processing of temporal differences in the sound input from both ears. Our results show that, in addition to synaptic remodeling and changes in postsynaptic receptors, changes in the neurotransmitter content of presynaptic terminals and their vesicles also contribute to the developmental switch from GABAergic to glycinergic inhibition in the rat LSO.

METHODS

All experiments were performed in accordance with the Guiding Principles for the Care and Use of Animals approved by the Council of the Physiological Society of Japan.

Electrophysiology. Wistar rats, at 1–17 d after birth (P1–P17), were quickly decapitated under ether anesthesia. Coronal midbrain slices containing the LSO were made (280-350 μm thickness) as previously described[36]. The ionic composition of the internal (patch pipette) solution for the whole-cell recordings contained 50 mM CsCl, 30 mM Cs_2SO_4, 0.5 mM $CaCl_2$, 2 mM $MgCl_2$, 5 mM EGTA, 5 mM TEA-Cl, 5 mM Mg-ATP and 10 mM HEPES. pH was adjusted to 7.2 with Tris-base. QX-314 (5 mM, Research Biochemicals) was added to the internal solution to block voltage-dependent Na^+ channels. The external solution for the brain slice recordings contained 124 mM NaCl, 5 mM KCl, 1.2 mM KH_2PO_4, 1.3 mM $MgSO_4$, 2.4 mM $CaCl_2$, 10 mM glucose, 24 mM $NaHCO_3$, and was well-oxygenated with 95% O_2/5% CO_2.

Single LSO neurons were mechanically dissociated from brain slices, so as to preserve functional presynaptic nerve terminals[15] (Fig. 2a). The internal patch-pipette solution for these recordings was as described above. The standard external solution contained 150 mM NaCl, 5 mM KCl, 1 mM $MgCl_2$, 2 mM $CaCl_2$, 10 mM HEPES and 10 mM glucose (pH 7.2). Antagonists and agonists were applied to acutely dissociated LSO neurons using a Y-tube perfusion device[37]. Neurons were pre-incubated with receptor antagonists for at least 30 s before recording data or applying agonists.

Spontaneous mIPSCs were acquired using pClamp 8.2 (Axon Instruments) and analyzed using both pClamp 8.2 and the MiniAnalysis program (Synaptosoft). Events were detected using an amplitude threshold of 2 pA and events were further rejected or accepted on the basis of their rise and decay times. Large numbers of mIPSCs (>200) were obtained from each neuron recording. mIPSC decay time constants were obtained by fitting a double exponential function to the mIPSC decay from the time period corresponding to between 90% and 10% of the peak mIPSC amplitude. Individual events were fitted (with >150 iterations) to the function: $y = y_0 + y_{fast}\, e^{(-x/\tau fast)} + y_{slow}\, e^{(-x/\tau slow)}$. mIPSCs where considered to have a mono-exponential decay when the relative contribution of one of the exponential distributions was <1%. Thus, the decision about whether a single mIPSC decayed with a single or dual components was completely objective. The proportion of GABAergic, glycinergic or mixed mIPSCs, in each recording, was automatically determined from the distribution of mIPSC decays. Numerical values are presented as means ± standard error of the mean (s.e.m.).

Post-embedding immunohistochemistry. Rats were deeply anesthetized with sodium pentobarbital (100 mg per kg body weight) and transcardially perfused with saline, followed by 15 min perfusion with fixative (a mixture of 2.5% glutaraldehyde and 4% paraformaldehyde in 0.1 M phosphate buffer). The brainstem was removed and incubated overnight (4 °C) in the same fixative. Subsequently, small blocks of brainstem, containing the LSO, were treated with 1% OsO_4, dehydrated in ethanol and propylene oxide, and embedded in Durcupan (ACM Fluka). Ultrathin slices were cut and mounted on nickel grids. Postembedding double immunogold labeling of GABA and glycine was performed as described[38]. The GABA antibody (1:8,000, gift of O.P. Ottersen, University of Oslo, Oslo, Norway) was visualized using an IgG coupled to 20 nm gold particles (GAR 20; 1:20, British Biocell International). The glycine antibody (1:1,000, Biogenesis) was visualized using a Fab fragment coupled to 10 nm gold particles (GFAR 10; 1:20, British Biocell International). The ultrathin specimens were initially incubated for GABA immunogold labeling, followed by that for glycine labeling. Specimens were exposed to formaldehyde vapor for 1 h at 80 °C to avoid any interference between the sequential incubations. Specimens only stained positive for the 20 nm gold-conjugated particles when they were incubated with the GABA-specific antibody while the smaller gold-conjugated particles were only observed when specimens contained the glycine-specific antibody (**Supplementary Fig. 2** online). The specificity of the antibodies under our conditions was tested[39]. Brain sections were processed alongside control sections containing a series of different amino acids glutaraldehyde-conjugated to brain macromolecules. For quantification of the amount of presynaptic glycine and GABA we manually counted the number of gold particles observed within presynaptic terminals that could be clearly seen to synapse onto the soma. Many terminals examined contained a low level of staining for GABA and glycine reactive gold particles (1–4 particles/μm^2). A second population contained a greater density of gold particles (**Supplementary Fig. 1** online). The presence of >5 particles/μm^2 was the only criteria used to accept inhibitory terminals for study. To compare particle density across different terminals and specimens, results are expressed as particles/μm^2. Three rats from each age group were used and the specimens derived from rats at the two different ages were grouped together. Sections contained terminals that synapsed on to the soma, or on the larger proximal dendrites.

Immunocytochemistry. Rats were deeply anesthetized with sodium pentobarbital (100 mg/kg body weight), and then were transcardially perfused with phosphate buffered saline (PBS, pH 7.4) followed by a mixture of 2% paraformaldehyde and 2.5% glutaraldehyde in 0.1 M phosphate buffer (pH 7.4). The brains were left *in situ* for 1–2 h at room temperature (22–24 °C) and then were removed from the skull. Small blocks containing the LSO were separated from the brain and then sliced transversely into 50 μm-thick serial sections. The thin sections were incubated in 30% sucrose in 0.1 M phosphate buffer (pH 7.4) for 1 h, and were then freeze-thawed in liquid nitrogen.

No detergents were used, as they can reduce the degree of glutamic acid decarboxylase (GAD) immunostaining. Slices were then incubated overnight in PBS containing 1% bovine serum albumin and 0.05% sodium azide, before being incubated in mixture of rabbit polyclonal anti-glycine antibody (1:10,000; Chemicon) and goat polyclonal S3 antibody against GAD (1:2,000; NIMH Laboratory of Clinical Science) for 5 d at 20 °C. The S3 antibody recognizes both GAD65 and GAD67 forms[40]. After this, the sections were rinsed briefly in PBS, and then incubated with a mixture of fluorescein isothiocyanate (FITC)-conjugated donkey anti-rabbit antibody (1:1,000; Jackson Immunoresearch) and rhodamine red-conjugated donkey anti-goat antibody (1:1,000; Jackson Immunoresearch) for 3 h. The sections were rinsed briefly in PB, mounted in Vectashield (Vector Laboratories) and examined with a confocal laser-scanning microscope (CLSM; TCS-SP2; Leica). Single laser beams, of 488 and 543 nm in wavelength, were alternately focused on to the specimen to collect fluorescent images for FITC (glycine) and rhodamine red (GAD), respectively. In the absence of the primary antibodies, only negligible background staining was observed in the LSO (data not shown), confirming the specificity of our GAD and glycine immunolabeling.

Note: Supplementary information is available on the Nature Neuroscience website.

ACKNOWLEDGMENTS

We thank A. Moorhouse for discussion and editing of the manuscript, and N. Akaike for technical advice. We also thank O.P. Otterson, I.J. Kopin, W.H. Oertel, D.E. Schmechel and M.L. Tappaz for help obtaining antibodies. This work was supported by research grants from the Ministry of Education, Culture, Sports, Science and Technology, Japan (15016082, 15650076 and 15390065 to J.N).

COMPETING INTERESTS STATEMENT

The authors declare that they have no competing financial interests.

Received 4 July; accepted 1 December 2003
Published online at http://www.nature.com/natureneuroscience/

1. Ornung, G. *et al.* Qualitative and quantitative analysis of glycine- and GABA-immunoreactive nerve terminals on motoneuron cell bodies in the cat spinal cord: a postembedding electron microscopic study. *J. Comp. Neurol.* **365**, 413–426 (1996).
2. Yang, H.W., Min, M.Y., Appenteng, K. & Batten, T.F. Glycine-immunoreactive terminals in the rat trigeminal motor nucleus: light- and electron-microscopic analysis of their relationships with motoneurones and with GABA-immunoreactive terminals. *Brain Res.* **749**, 301–319 (1997).
3. Levi, S., Chesnoy-Marchais, D., Sieghart, W. & Triller, A. Synaptic control of glycine and $GABA_A$ receptors and gephyrin expression in cultured motoneurons. *J. Neurosci.* **19**, 7434–7449 (1999).
4. Kneussel, M. & Betz, H. Receptors, gephyrin and gephyrin-associated proteins: novel insights into the assembly of inhibitory postsynaptic membrane specializations. *J. Physiol.* **525**, 1–9 (2000).
5. O'Brien, J.A. & Berger, A.J. Cotransmission of GABA and glycine to brain stem motoneurons. *J. Neurophysiol.* **82**, 1638–1641 (1999).
6. Jonas, P., Bischofberger, J. & Sandkuhler, J. Co-release of two fast neurotransmitters at a central synapse. *Science* **281**, 419–424 (1998).
7. Russier, M., Kopysova, I.L., Ankri, N., Ferrand, N. & Debanne, D. GABA and glycine co-release optimizes functional inhibition in rat brainstem motoneurons *in vitro*. *J. Physiol.* **541**,123–137 (2002).
8. Kotak, V.C., Korada, S., Schwartz, I.R. & Sanes, D.H. A developmental shift from GABAergic to glycinergic transmission in the central auditory system. *J. Neurosci.* **18**, 4646–4655 (1998).
9. Smith, A.J., Owens, S. & Forsythe, I.D. Characterization of inhibitory and excitatory postsynaptic currents of the rat medial superior olive. *J. Physiol.* **529**, 681–698 (2000).
10. Sanes, D.H. & Friauf, E. Development and influence of inhibition in the lateral superior olivary nucleus. *Hear. Res.* **147**, 46–58 (2000).
11. Korada, S. & Schwartz, I.R. Development of GABA, glycine, and their receptors in the auditory brainstem of gerbil: a light and electron microscopic study. *J. Comp. Neurol.* **409**, 664–681 (1999).
12. del Castillo, J. & Katz, B. Quantal components of end-plate potential. *J. Physiol.* **124**, 560–573 (1954).
13. Walmsley, B., Alvarez, F.J. & Fyffe, R.E. Diversity of structure and function at mammalian central synapses. *Trends Neurosci.* **21**, 81–88 (1998).
14. Akaike, N. & Moorhouse, A.J. Techniques: applications of the nerve-bouton preparation in neuropharmacology. *Trends Pharmacol. Sci.* **24**, 44–47 (2003).
15. Dumoulin, A., Triller, A. & Dieudonne, S. IPSC kinetics at identified GABAergic and mixed GABAergic and glycinergic synapses onto cerebellar Golgi cells. *J. Neurosci.* **21**, 6045–6057 (2001).
16. Keller, A.F., Coull, J.A., Chery, N., Poisbeau, P. & De Koninck, Y. Region-specific developmental specialization of GABA-glycine cosynapses in laminas I-II of the rat spinal dorsal horn. *J. Neurosci.* **21**, 7871–7880 (2001).
17. Friauf, E, Hammerschmidt, B. & Kirsch, J. Development of adult-type inhibitory glycine receptors in the central auditory system of rats. *J. Comp. Neurol.* **385**, 117–134 (1997).
18. Otis, T.S., De Koninck, Y. & Mody, I. Lasting potentiation of inhibition is associated with an increased number of gamma-aminobutyric acid type A receptors activated during miniature inhibitory postsynaptic currents. *Proc. Natl. Acad. Sci. USA* **91**, 7698–7702 (1994).
19. Sanes, D.H. & Siverls, V. Development and specificity of inhibitory terminal arborizations in the central nervous system. *J. Neurobiol.* **22**, 837–854 (1991).
20. Kim, G. & Kandler, K. Elimination and strengthening of glycinergic/GABAergic connections during tonotopic map formation. *Nat. Neurosci.* **6**, 282–290 (2003).
21. Gasnier, B. The loading of neurotransmitters into synaptic vesicles. *Biochimie* **82**, 327–337 (2000).
22. Schotzinger, R.J. & Landis, S.C. Cholinergic phenotype developed by noradrenergic sympathetic neurons after innervation of a novel cholinergic target *in vivo*. *Nature* **335**, 637–639 (1988).
23. Habecker, B.A., Tresser, S.J., Rao, M.S. & Landis, S.C. Production of sweat gland cholinergic differentiation factor depends on innervation. *Dev. Biol.* **167**, 307–316 (1995).
24. Rietzel, H.J. & Friauf, E. Neuron types in the rat lateral superior olive and developmental changes in the complexity of their dendritic arbors. *J. Comp. Neurol.* **390**, 20–40 (1998).
25. Takahashi, T., Momiyama, A., Hirai, K., Hishinuma, F. & Akagi, H. Functional correlation of fetal and adult forms of glycine receptors with developmental changes in inhibitory synaptic receptor channels. *Neuron* **9**, 1155–1161 (1992).
26. Kakazu, Y., Akaike, N., Komiyama, S. & Nabekura, J. Regulation of intracellular chloride by cotransporters in developing lateral superior olive neurons. *J. Neurosci.* **19**, 2843–2851 (1999).
27. Kandler, K. & Friauf E. Development of glycinergic and glutamatergic synaptic transmission in the auditory brainstem of perinatal rats. *J. Neurosci.* **15**, 6890–6904 (1995).
28. Balakrishnan, V. *et al.* Expression and function of chloride transporters during development of inhibitory neurotransmission in the auditory brainstem. *J. Neurosci.* **23**, 4134–4145 (2003).
29. Kullmann, P.H., Ene, F.A. & Kandler, K. Glycinergic and GABAergic calcium responses in the developing lateral superior olive. *Eur. J. Neurosci.* **15**, 1093–1104 (2002).
30. Gao, B.X. & van den Pol, A.N. GABA, not glutamate, a primary transmitter driving action potentials in developing hypothalamic neurons. *J. Neurophysiol.* **85**, 425–434 (2001).
31. Ganguly, K., Schinder, A.F., Wong, S.T. & Poo, M. GABA itself promotes the developmental switch of neuronal GABAergic responses from excitation to inhibition. *Cell* **105**, 521–532 (2001).
32. Lauder, J.M., Liu, J., Devaud, L. & Morrow, A.L. GABA as a trophic factor for developing monoamine neurons. *Perspect. Dev. Neurobiol.* **5**, 247–259 (1998).
33. Kirsch, J. & Betz, H. Glycine-receptor activation is required for receptor clustering in spinal neurons. *Nature* **392**, 717–720 (1998).
34. Kotak, V.C., DiMattina, C. & Sanes, D.H. $GABA_B$ and Trk receptor signaling mediates long-lasting inhibitory synaptic depression. *J. Neurophysiol.* **86**, 536–540 (2001).
35. Chang, E.H., Kotak, V.C. & Sanes, D.H. Long-term depression of synaptic inhibition is expressed postsynaptically in the developing auditory system. *J. Neurophysiol.* **90**, 1479–1788 (2003).
36. Kakazu, H., Uchida, S., Nakagawa, T., Akaike, N. & Nabekura, J. Reversibility and cation selectivity of K^+-Cl^- cotransport in rat CNS Neurons. *J. Neurophysiol.* **84**, 281–288 (2000).
37. Nabekura J., Omura T. & Akaike N. Alpha2 adrenoceptor potentiates glycine receptor-mediated taurine response through protein kinase A in rat substantia nigra neurons. *J. Neurophysiol.* **76**, 2447–2454 (1996).
38. Matsubara, A., Laake, J.H., Davanger, S., Usami, S. & Ottersen, O. P. Organization of AMPA receptor subunits at a glutamate synapse: a quantitative immunogold analysis of hair cell synapses in the rat organ of Corti. *J. Neurosci.* **16**, 4457–4467 (1996).
39. Ottersen, O.P., Zhang, N. & Walberg, F. Metabolic compartmentation of glutamate and glutamine morphological evidence obtained by quantitative immunocytochemistry in rat cerebellum. *Neuroscience* **46**, 519–534 (1992).
40. Kaufman, D.L., McGinnis, J.F., Krieger, N.R. & Tobin, A.J. Brain glutamate decarboxylase cloned in lambda gt-11: fusion protein produces gamma-aminobutyric acid. *Science* **232**, 1138–1140 (1986).

Available online at www.sciencedirect.com
SCIENCE DIRECT®
Neuroscience Research 48 (2004) 211–220
Neuroscience Research
www.elsevier.com/locate/neures

Experience-dependent changes in intracellular Cl^- regulation in developing auditory neurons

Shumei Shibata[a], Yasuhiro Kakazu[a], Akihito Okabe[b], Atsuo Fukuda[b], Junichi Nabekura[a,*]

[a] *Department of Cellular and System Physiology, Graduate School of Medical Sciences, Kyushu University, Fukuoka 812-8582, Japan*
[b] *Department of Physiology, Hamamatsu University School of Medicine, Hamamatsu 420-3192, Japan*

Received 21 August 2003; accepted 29 October 2003

Abstract

A developmental change in GABA and glycine responses, from a depolarization to a hyperpolarization, have been reported for a range of CNS neurons, and has been demonstrated to be due to a developmental decrease in the intracellular Cl^- concentration ($[Cl^-]_i$). We examined $[Cl^-]_i$ in isolated rat lateral superior olive (LSO) neurons using patch-clamp recordings of glycine gated Cl^- currents and by measuring intracellular Cl^--fluorescence. In neurons from 14–16-day-old rats (P14–P16), which had previously received unilateral or bilateral cochlear ablations before the onset of hearing, there was no developmental decrease in $[Cl^-]_i$. No significant differences in $[Cl^-]_i$ were observed amongst rats with either ipsi- and contralateral ablations. Implanted strychnine pellets also prevented the decrease in $[Cl^-]_i$ in most neurons. In some of these neurons in which $[Cl^-]_i$ remained high, there was a lack of expression of the K^+–Cl^- cotransporter 2 (KCC2) mRNA. These results demonstrate that the developmental decrease in $[Cl^-]_i$ in LSO neurons is dependent on neuronal activity and that both GABAergic/glycinergic and glutamatergic afferent activity contribute to this maturation of the Cl^- regulatory mechanisms.

Keywords: Development; Ablation; KCC2; LSO; Auditory brainstem; Perforated-patch clamp; RT-PCR

1. Introduction

Many studies have indicated that excitatory neuronal circuits can be modified by sensory experiences (Wiesel and Hubel, 1963; Klinke et al., 1999; Rittenhouse et al., 1999; Di Cristo et al., 2001). There are also reports that inhibitory circuits are also adversely affected when sensory input is disrupted. In the visual and auditory systems, for example, deafferentation affects the development of appropriate inhibitory neuronal circuits (Hensch et al., 1998; Rajan, 1998; Mossop et al., 2000; Kapfer et al., 2002).

Deafferentation can also affect the subsequent properties of synaptic transmission across surviving synapses. At many immature synapses, activation of GABA or glycine receptor channels can evoke a membrane depolarization mediated by Cl^- efflux and resulting from a high intracellular Cl^- concentration ($[Cl^-]_i$) (Cherubini et al., 1991; Luhmann and Prince, 1991; Chen et al., 1996; Kaila, 1994; Rohrbough and Spitzer, 1996; Hollrigel and Soltesz, 1997). With maturation, $[Cl^-]_i$ becomes lower, and GABA and glycine typically cause a Cl^- influx and a hyperpolarization in mature neurons. Changes in $[Cl^-]_i$ throughout development are thought to be mediated by a developmental change in Cl^- transport proteins, which include the Na^+–K^+–Cl^- and K^+–Cl^- cotransporters (NKCC and KCC, respectively), and the Cl^-–HCO_3^- and Na^+–Cl^-–HCO_3^- exchangers (Kaila, 1994; Payne et al., 2003). Among these Cl^- transporters, a developmental up-regulation of the K^+–Cl^- cotransporter has been suggested to be responsible for the developmental decrease in $[Cl^-]_i$ (Rivera et al., 1999; Kakazu et al., 1999). In the inferior colliculus, bilateral cochlea ablations cause the reversal potential of evoked inhibitory postsynaptic currents (IPSCs) to remain at a more depolarized level (Vale and Sanes, 2000, 2002). The ablations also reduced the ability of neurons to transport Cl^-, although the levels of NKCC1 and KCC2 mRNA were unchanged (Vale et al., 2003). Bilateral ablations also reduced the postsynaptic conductance change associated with the IPSC, affected presynaptic

* Corresponding author. Tel.: +81-92-642-6090; fax: +81-92-642-6094.
E-mail address: nabekura@physiol2.med.kyushu-u.ac.jp (J. Nabekura).

0168-0102/$ – see front matter
doi:10.1016/j.neures.2003.10.011

transmitter release and altered excitatory transmission in the inferior colliculus (Vale and Sanes, 2000, 2002). Just how deafferentiation leads to these changes is not clear.

The lateral superior olive (LSO) is the first auditory center involved in processing the different sound intensity experienced by the two ears (Sanes, 1993; Koyano and Ohmori, 1996). The LSO receives glutamatergic innervations directly from the ipsilateral cochlea nucleus, and GABA/glycinergic inputs from the contralateral cochlear nucleus via the medial nucleus of the trapezoid body (MNTB) (Grothe et al., 1994; Suneja et al., 1995; Vater, 1995; Winer et al., 1995; Kotak et al., 1998). Cochlea ablations in the first postnatal week have been shown to alter the morphology of LSO neurons and their inhibitory inputs (Sanes et al., 1992; Sanes and Chokshi, 1992). Contralateral cochlear ablation in immature gerbils, as well as in vivo application of strychnine, both of which should preferentially deafferentiate inhibitory inputs, disrupts the developmental refinement of LSO dendrites (Sanes and Takacs, 1993).

In this study, we investigate the effects of auditory experience on Cl^- homeostasis and KCC2 expression, in rat lateral superior olive neurons. We were particularly interested in whether just inhibitory input from the contralateral cochlea was sufficient to sustain the typical changes in $[Cl^-]_i$ and IPSCs seen during LSO development. We have also investigated whether there is any correlation between $[Cl^-]_i$ and the levels of KCC2.

2. Methods

2.1. Cochlea ablations and hearing tests

Bilateral and unilateral cochlear ablations were performed at P7. Rats were anesthetized with diethyl ether, and an incision was made just behind the pinna. Under a dissecting microscope, the middle ear cavity was exposed and the bony wall of the cochlea was identified. The cochlea was then carefully destroyed using a needle. Control sham-operated rats only received the incisions behind the pinna. After suturing the incision, we placed the animals on a heating pad until recovery from anesthesia was complete after which the pups were returned to their original cages and reared until P14.

At P14, the extent of hearing was tested by measurements of the auditory brainstem response (ABR) (Morishita et al., 2001). Briefly, rats were first anesthetized with injection of pentobarbital (60 mg/kg of body mass) and subcutaneous needle electrodes were placed at the vertex of the head, in the right and left retro-auricular region, and in the pre-sacral region of the rats. The sound stimulus was a 1 ms burst of 75 dB clicks presented at 5 kHz clicks (duration of each click was 0.1 ms), delivered to the rats through a probe designed to fit the external ear canal. For each recording condition, responses to 1000 bursts of clicks were averaged. All tests were performed in a soundproof room and the ABR was recorded with a SYNAX ER1100 system (NEC, Japan). The sound intensity through the probe was calibrated by a sound pressure meter (NL-04, Rion). The stimuli were delivered to control and test rats derived from the same litter.

2.2. Strychnine implants

To pharmacologically block glycinergic inputs, we implanted slow release strychnine pellets (i.e. strychnine-rearing). These strychnine pellets (0.05 mg 21-day-release, Innovative Research of America, Toledo, OH) were implanted subcutaneously at a posterior mid-dorsal location (Kotak and Sanes, 1996). Implantations were performed at P3, because rats suffered from general seizure when pellets were embedded at ages older than P5. After implantation, rats were returned to their litter.

2.3. Preparation of slices and acute dissociation of LSO neurons

Acute dissociation of central neurons was as described previously (Nabekura et al., 1996). Wister rats between P0–P3 or between P14–P16, either with or without cochlea ablation, or with strychnine pellets, were quickly decapitated under ether anesthesia and the brain was rapidly excised and immersed in ice-cold standard solution (below). Approximately 400 μm slices were cut using a vibratome (VT1000, Leica) and incubated in standard solution at room temperature for 1 h before a single slice was transferred to a petri dish and observed under the light microscope. Fine glass pipettes were placed on the surface of the LSO and gently vibrated so as to liberate single, mechanically dissociated LSO neurons. The dissociated LSO neurons were left for about 10 min to adhere to the bottom of the Petri dish before commencing electrophysiological recordings.

2.4. Solutions

The standard solution contained: NaCl, 150 mM; KCl, 5 mM; $MgCl_2$, 1 mM; $CaCl_2$, 2 mM; glucose, 10 mM and HEPES, 10 mM (pH = 7.4 with Tris-base). The artificial cerebrospinal fluid (ACSF) solution contained: NaCl, 124 mM; KCl, 5 mM; KH_3PO_4, 1.2 mM; $MgSO_4$, 1.3 mM; $CaCl_2$, 2.4 mM; glucose, 10 mM and $NaHCO_3$, 24 mM (pH = 7.45 with 95% O_2 and 5% CO_2). The pipette solution for the gramicidin perforated patch-clamp recordings contained: KCl, 150 mM; HEPES, 10 mM (pH = 7.2 with Tris-base). Gramicidin D, purchased from Sigma (USA), was dissolved in methanol as a 10 mg/ml stock solution, and this stock solution was diluted in the pipette solution to the given concentration. As the effectiveness of the diluted gramicidin stock solution gradually declined over time, it was prepared just before each experiment, and was only used for up to a maximum of 5 h.

2.5. Electrophysiological recordings

All electrical recordings utilized the gramicidin perforated patch-clamp technique. Membrane currents and voltages were continuously measured with a patch-clamp amplifier (EPC-7, List-Electronic), low pass filtered at 1 kHz (FV-665, NF Electronic Instruments), and monitored on both an oscilloscope (HS-5100A, Iwatsu) and a pen recorder (RECTI-HORIZ-8K21, Nihondenki San-ei). Data were simultaneously recorded on videotapes after digitalization (at 5 kHz) with a PCM processor (PCM 501 ESN, Nihon Koden). Patch pipettes were made from glass capillaries (outer diameter 1.5 mm) using a vertical pipette puller (PB-7, Narishige Scientific Instruments). The tip resistance was 4–8 MΩ. Voltage offsets were nulled before formation of the GΩ seal. After making contact with the cell surface, a GΩ seal was established by applying gentle suction to the patch pipette interior. After the cell attached configuration had been attained, the pipette potential was set to −50 and −10 mV hyperpolarizing step pulses were periodically delivered to monitor the access resistance. The access resistance typically reached a steady level below 20 MΩ within 40 min after making the GΩ seal. In all experiments, 75–80% series resistance compensation was employed. All experiments were carried out at 28–30 °C.

2.6. Drug application

External solutions were applied to single neurons using a "Y-tube" (Nabekura et al., 1993). Using this technique, solutions could be completely exchanged within 10–20 ms.

2.7. Drugs

Drugs used in the experiments were gramicidin D (Sigma, USA), glycine (Kanto, Japan; Tokyo Kasei, Japan), tetrodotoxin (TTX) (Sankyo, Japan). Final drug concentrations were made up from stock solutions just before use.

2.8. Optical imaging of intracellular Cl^-

The highly membrane permeant compound DiH-MEQ, was produced by reducing MEQ (Fukuda et al., 1998). Briefly, under protection from light, 5 mg of MEQ was dissolved in 100 μl of distilled water gassed with 100% N_2. The dissolved MEQ was reduced by addition of 15 μl of 12% $NaBH_4$. DiH-MEQ was extracted from the reaction mixture as a yellow organic layer with the aid of diethyl ether. This organic layer was dehydrated using 100 mg of $MgSO_4$ for 5 min, and the ether was then evaporated under a stream of 100% N_2 in a glass test tube. A portion of the organic extract was dissolved in 15 μl of ethyl acetate and added to the ACSF to yield a final concentration of 740 μM diH-MEQ.

Neurons were loaded with MEQ by incubating slices with diH-MEQ (740 μM) in ACSF for 60–90 min. DiH-MEQ is Cl^--insensitive, but it is readily loaded into cells where it is readily oxidized in the cytosol to form MEQ, which is both Cl^--sensitive and membrane impermeable (Biwersi and Verkman, 1991). The MEQ remains trapped in the cytosol for several hours. Pre-incubated slices were laid on the glass bottom of a submerged-type chamber, placed on a microscope stage and continuously perfused at a rate of 3–4 ml/min with ACSF.

For calibration of MEQ fluorescence we used ACSF solutions containing different Cl^- concentrations, in which the NaCl was replaced with equimolar concentrations of K gluconate.

MEQ fluorescence was excited at 330 nm (and emitted at 450 nm) using a Xenon arc lamp (75 W) and a band pass filter set. Fluorescence images were obtained using a CCD camera (Cool Snap cf., Roper Scientific) fitted to an upright microscope (DIA PHOT 300, Nikon). Images were digitized on-line, 128 frames being averaged to improve the signal to noise ratio. Data were analyzed using an image processor and data analysis software (MetaMorph/MetaVue, Roper Scientific). The apparent leakage and/or bleaching of MEQ under the recording conditions described here, was indicated by a gradual and linear decline in fluorescence, and was about 10–30% after 30 min. MEQ fluorescence was measured in the center of the soma of LSO neurons, once every 6–10 s. MEQ fluorescence was normalized to that initially observed, and plotted against time. Drugs were applied to the slices by bath perfusion.

2.9. Single-cell multiplex RT-PCR analysis

For harvesting cell cytoplasm for subsequent single-cell multiplex RT-PCR reactions, 10 μl of the standard pipette solution was injected into each patch-clamp pipette. After completion of the whole cell recording, mild suction was used to aspirate the contents of the cell into the recording pipette tip which were then expelled into a microfuge tube. The harvested cytoplasm was frozen with crushed dry ice and stored at −80 °C for a maximum of 2 days. Several target sequences were simultaneously amplified from a single cDNA synthesis by multiplex PCR with nested primers (below) and with two rounds of amplification. RT and first-round PCR reactions took place in the same tube using a OneStep RT-PCR kit (QIAGEN, GmbH). PCR analysis was carried out to determine the presence of β-actin and Cl^- transport proteins. For the initial RT-PCR, 10 μl of pipette solution containing the cell cytoplasm was placed into a thin-walled PCR tube and to this was added 10 μl of Qiagen OneStep RT-PCR buffer (5×), 2 μl of Qiagen OneStep RT-PCR enzyme mix, 0.4 mM of dNTP, 8 units of RNase inhibitor (Promega, Tokyo, Japan) and 0.6 μM of each primer, made up in buffer supplied by the manufacturer and added to give a final reaction volume of 50 μl. After the RT reaction at 50 °C for 30 min, the first-round PCR was subsequently performed in the same tube with a 15 min pre-incubation at 95 °C followed by 40 cycles of 30 s at 94 °C (denaturation),

30 s at 55 °C (annealing), 1 min at 72 °C (extension) in Program Temp Control System (PC-801, ASTEC Co. Ltd., Fukuoka, Japan). Subsequently, first-round PCR products were diluted 25-fold and re-amplified for 40 cycles (94 °C, 30 s; 60 °C, 30 s; 72 °C, 1 min) in separate reactions using the internal primer pairs for each template. The second-round PCR reaction was performed with 5 μl PCR buffer (10×), 3 mM $MgCl_2$, 0.2 mM of each dNTP (Amersham Bioscience, Tokyo, Japan), 1.25 units HotStar-Taq DNA polymerase (QIAGEN, GmbH) in the buffer supplied with enzyme and a reaction volume of 50 μl. The solution containing cDNA products was subjected to 10% acrylamide gel electrophoresis with ethidium bromide.

2.10. PCR primers

Nested primers used for the PCR analyses were selected based on the known rat cDNA or genomic sequences and are listed below. The outside primer pair is listed first in each case; the size of the final amplification product is shown in parentheses:

KCC2 (GenBank # U55816, Gillen et al., 1996), 5′-GATGAAGAAAGACCTGACCA-3′/5′-CTGGTTCAAGTTTTCCCACT-3′ and 5′-CATTCGGAGGAAGAATCCAG-3′/5′-TTTGTTCTTCTGAGCCGCTG-3′ (238 bp; 2935–3172 bp); β-actin (GenBank # V01217, Nudel et al., 1983), 5′-ACACGGCATTGTAACCAACT-3′/5′-CATTGCCGATAGTGATGACC-3′ and 5′-AGAAGATTTGGCACCACACT-3′/5′-CCATCTCTTGCTCGAAGTCT-3′ (435 bp).

3. Results

3.1. Developmental changes in $[Cl^-]_i$ in LSO neurons

In the present study, we used gramicidin perforated patch-clamp recordings from LSO neurons acutely dissociated from rats aged between P0–P2 and P14–P16. The gramicidin pore allows permeation of monovalent cations but does not allow anion permeation and hence the physiological $[Cl^-]_i$ is maintained (e.g., Kakazu et al., 1999). We measured the response to glycine at different membrane potentials and considered that E_{Gly} was close to the Cl^- equilibrium potential. The intracellular Cl^- concentration ($[Cl^-]_i$) could then be estimated using the Nernst equation (e.g., Kakazu et al., 1999). In neurons isolated from P0–P2 rats, with a large number of LSO neurons containing a relatively high $[Cl^-]_i$, there was a wide range of $[Cl^-]_i$, from between about 5–45 mM, with a mean value of 19.6 ± 1.8 mM (n = 37) (Fig. 1Aa). For almost all neurons from P16 rats, however, $[Cl^-]_i$ was below 10 mM with a mean value of 7.9 ± 0.3 mM, significantly lower than in the immature neurons ($P < 0.01$) (Fig. 1Ab). These results show that there is a fall in $[Cl^-]_i$ in LSO neurons during

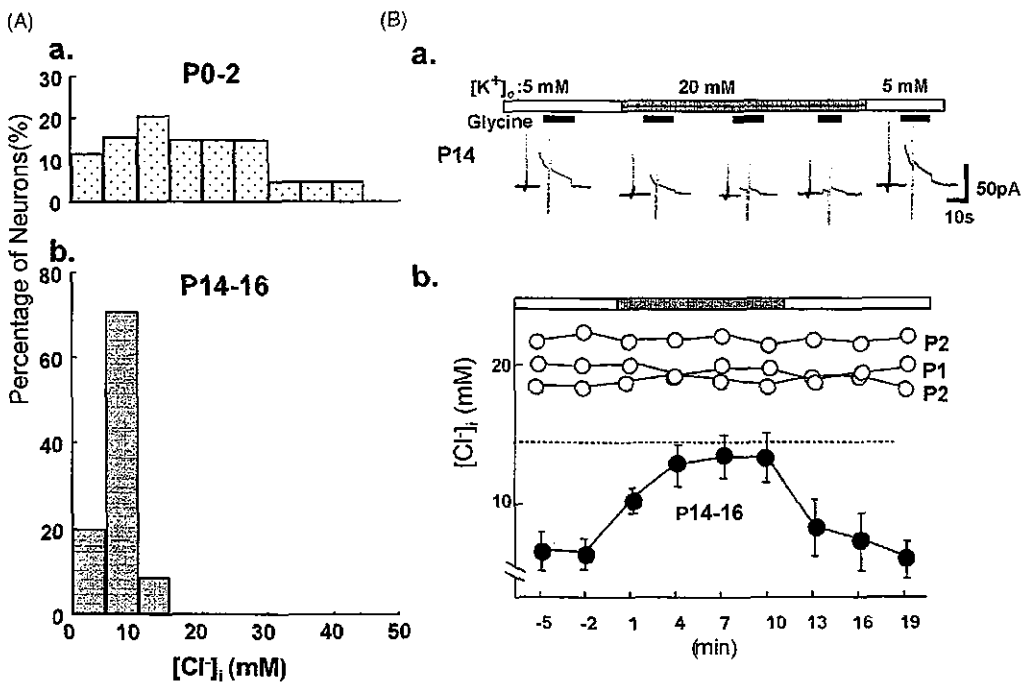

Fig. 1. Developmental increase in K^+-dependent Cl^- extrusion in LSO neurons. (A) Distribution of $[Cl^-]_i$ in LSO neurons, isolated from P0–P2 rats (upper, n = 37) and P14–P16 (lower, n = 37). Note the larger number of neurons with a relatively high $[Cl^-]_i$ in the P0–P2 neurons, while in P14–P16 neurons $[Cl^-]_i$ was typically below 10 mM. (B(a)) K^+-dependent Cl^- extrusion in mature LSO neurons at P14. V_H was −50 mV. An increase in $[K^+]_o$ from 5 to 20 mM abolished outward currents. The vertical current transients in current traces are in response to voltage ramps applied during the glycine response. (B(b)) $[Cl^-]_i$ in LSO neurons from P0–P2 (open circles) and from P14–P16 rats (filled circles, mean ± S.E.M., n = 6–12) before, during and after application of 20 mM $[K^+]$.

the first two postnatal weeks, and this results in a switch of glycine responses from excitatory to inhibitory.

3.2. Regulation of $[Cl^-]_i$ by cation-chloride cotransporters during development

Several studies have demonstrated that the K^+–Cl^- cotransporter (KCC) plays an important role in this developmental decrease in $[Cl^-]_i$, including in the LSO (Rivera et al., 1999; Kakazu et al., 1999). We also investigated the involvement of KCC in the present study, by altering its activity by manipulating the K^+ driving force across the plasma membrane. An increase in the extracellular K^+ concentration ($[K^+]_o$) is expected to cause a decrease in the ability of KCC to cotransport Cl^- and K^+ from inside cells. We monitored changes in $[Cl^-]_i$ by repetitively evoking glycinergic currents, which also causes some Cl^- loading into the cell at a V_H of −50 mV (e.g., Thompson and Gahwiler, 1989; Haas and Forbush, 1998; Kakazu et al., 2000; Ueno et al., 2002).

In neurons from P14–P16 rats, an increase in extracellular K^+ concentration ($[K^+]_o$) from 5 to 20 mM resulted in a gradual reduction in the amplitude of outwardly directed I_{Gly} evoked at a V_H of −50 mV (Fig. 1B). During perfusion with 20 mM $[K^+]_o$, $[Cl^-]_i$ was estimated from E_{Gly} to gradually increase to a significantly higher level than observed in the presence of 5 mM $[K^+]_o$ (Fig. 1B; $n = 5$; $P < 0.01$; paired t-test). At a V_H of −50 mV, I_{Gly} changed from an outward to an inward current in the presence of 30 mM $[K^+]_o$ (data not shown, see also Kakazu et al., 1999). After $[K^+]_o$ was returned from 20 to 5 mM, $[Cl^-]_i$ gradually recovered back to control values. This result indicates that $[K^+]_o$-dependent mechanism plays an important role in extruding Cl^- at P13–P15. In contrast, the initially higher $[Cl^-]_i$ in neurons from P0–P2 rats was less affected by a change in $[K^+]_o$ (Fig. 1Bb), indicating that this $[K^+]_o$-dependent $[Cl^-]_i$ regulation is not well developed in LSO neurons at this age (see also Kakazu et al., 1999).

3.3. Auditory activity alters the developmental changes in $[Cl^-]_i$

The hearing ability of rats was tested by recording the auditory brainstem response. Up until the age of P9, no ABR was observed in response to a 75 dB click, as previously reported (Geal-Dor et al., 1993). At P14 rats responded to the 75 dB click with a clear ABR (Fig. 2B, upper panel). In contrast, rats that received bilateral cochlear ablation at P7 showed no ABR at P14–P16 (Fig. 2B, middle panel). In rats who received a unilateral cochlear ablation at P7, the ABR in response to a click presented to the ear with cochlear ablation was diminished in amplitude, but the intact ear still showed a clear ABR (Fig. 2B, lower panel).

We next addressed the question whether auditory-dependent activity might influence the developmental decrease in the intracellular Cl^- concentration. Bilateral cochlear ablations or sham control operations were performed at P7. When neurons were subsequently isolated at P14, a significantly greater proportion of neurons from the cochlear ablation rats had a high $[Cl^-]_i$ when compared to those from the control rats ($P < 0.01$, Mann–Whitney test)(Fig. 3).

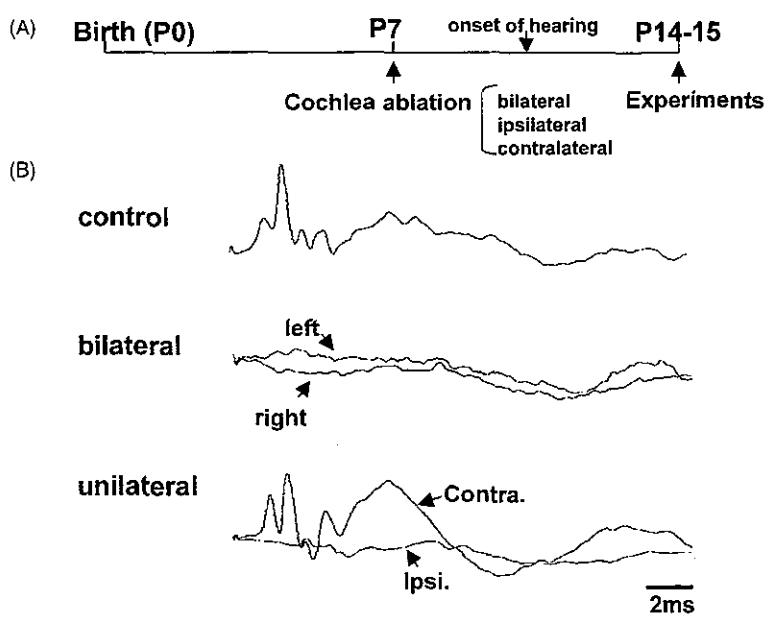

Fig. 2. Effects of cochlea ablation on the auditory brainstem responses. (A) Time line of experimental protocol. At P7, before the onset of hearing (P10–P12), bilateral or unilateral cochlea ablations, or sham control operations, were performed and auditory brainstem responses (ABR) were obtained at P14–P15. (B) ABRs recorded from control rats (upper trace), from rats with bilateral ablation in response to input to the left and right ears (center traces) and from rats with unilateral ablation in response to input to the ipsilateral and contralateral ears (lower traces). No response to sound stimuli applied to a cochlea-ablated ear were obtained.

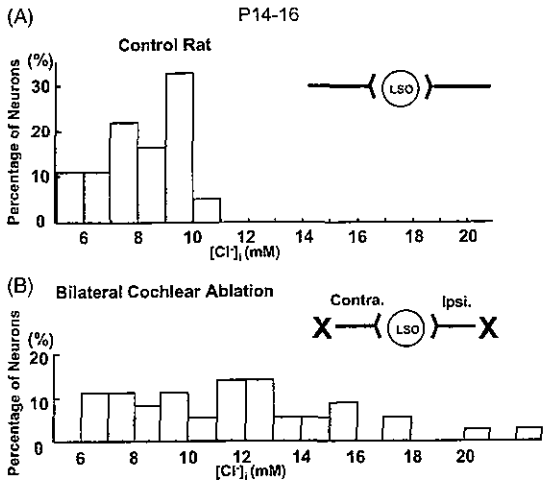

Fig. 3. Intracellular Cl^- concentration in LSO neurons from P14–P16 rats with sham and bilateral cochlear ablations performed at P7. Histograms showing the distribution of $[Cl^-]_i$ in LSO neurons from P14–P16 rats, with control (shame-operated, A) or bilateral cochlear ablations (B). $[Cl^-]_i$ was significant higher in the bilateral ablated rats, with a mean value of 11.6 ± 0.6 mM ($n = 32$) than in the sham control operated rats, with a mean value of 8.2 ± 0.2 mM ($n = 36$) ($P < 0.01$, Mann–Whitney test).

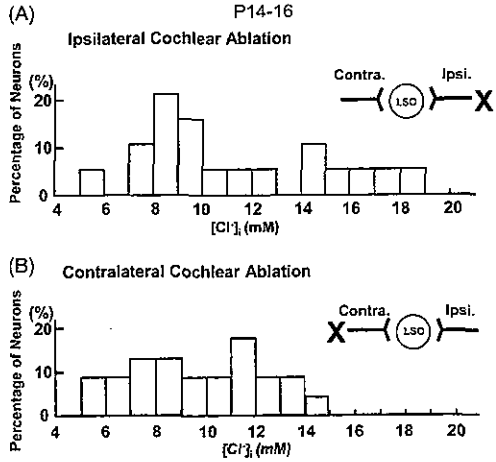

Fig. 4. Intracellular Cl^- concentration in LSO neurons from P14 rats with ipsi- or contralateral cochlear ablations performed at P7. Histograms showing the distribution of $[Cl^-]_i$ in LSO neurons from P14–P16 rats, with ipsilateral cochlea ablations (A) or contralateral cochlear ablations (B). For both groups, $[Cl^-]_i$ was significant higher (ipsi- 11.3 ± 0.9 mM, $n = 19$; contra- 9.8 ± 0.6 mM, $n = 23$) than in control (Fig. 3A) but there was no significant difference in the $[Cl^-]_i$ distribution between the ipsi- or contralateral ablations.

This indicates that the developmental decrease in intracellular Cl^- concentration is affected by auditory experience. On the other hand, $[Cl^-]_i$ in the bilateral ablation group (Fig. 3B) was significantly lower than $[Cl^-]_i$ in P0–P2 rats (Fig. 1Aa, $P < 0.05$), indicating that the developmental change in $[Cl^-]_i$ can proceed in the absence of auditory input and is accelerated by auditory experience.

We next investigated whether the ipsilateral auditory input (which sends glutamatergic afferents to the LSO) or the contralateral auditory input (involving GABAergic and glycinergic afferents) (Kotak et al., 1998) was predominantly responsible for the effects of the bilateral ablations. We performed unilateral cochlear ablations at P7 and recorded I_{GLY} in neurons isolated from the ipsilateral or contralateral LSO at P14–P16. Ablation of either the ipsilateral or contralateral cochlea both significantly affected the normal developmental decrease in $[Cl^-]_i$ ($P < 0.05$ contralateral ablation versus control; $P < 0.01$ ipsilateral ablation versus control) (Fig. 4). There appeared to be a larger number of neurons with $[Cl^-]_i > 15$ mM in neurons with an ablated ipsilateral input (Fig. 4), although there was no significant difference in the $[Cl^-]_i$ between neurons with ipsilateral, contralateral or bilateral ablations.

Finally, we examined the involvement of glycinergic neurotransmission in the developmental decrease in $[Cl^-]_i$ by using chronic in vivo blockade of glycine receptors with implanted strychnine pellets, which has previously been shown to disturb the morphological development of LSO neurons (Sanes and Chokshi, 1992). A significantly larger proportion of LSO neurons isolated from strychnine-reared rats at P14–P16 had a high $[Cl^-]_i$, when compared to neurons from control rats (Fig. 5A, $P < 0.05$). We also confirmed that strychnine-rearing attenuated the developmental decrease in $[Cl^-]_i$ using optical imaging with the Cl^- sensitive dye, MEQ (Fukuda et al., 1998). In LSO neurons in slices from P15 control rats, application of glycine elicited a decrease in MEQ fluorescence, indicating an increase in $[Cl^-]_i$ in response to glycine application (Fig. 5A). In contrast, application of glycine to LSO neurons in slices from strychnine-reared P15 rats, an increase in fluorescence was more typically seen in response to glycine, suggesting an efflux of Cl^- in response to glycine, consistent with an elevated initial $[Cl^-]_i$ (Fig. 5B). There was also typically a lower level of basal MEQ fluorescence in neurons from strychnine-reared rats, as compared to control neurons, which is also consistent with their higher basal $[Cl^-]_i$.

3.4. Developmental changes in KCC2 mRNA expression

Among the various KCC isoforms, KCC2 is neuron specific and changes in its function and/or expression have been shown to play a major role in the developmental decrease of $[Cl^-]_i$ (Rivera et al., 1999) and in the diversity of $[Cl^-]_i$ among neurons from various brain regions (Ueno et al., 2002). Therefore we performed single-cell RT-PCR to investigate any developmental change in KCC2 mRNA expression. We found that every LSO neuron isolated from P13–P16 rats expressed KCC2, while only two of seven LSO neurons from P0–P3 rats expressed KCC2. β-Actin was expressed at comparable levels in all neurons at both ages. In an additional set of experiments, we investigated whether there was a correlation between the $[Cl^-]_i$ concentration estimated during gramicidin perforated-patch recordings and

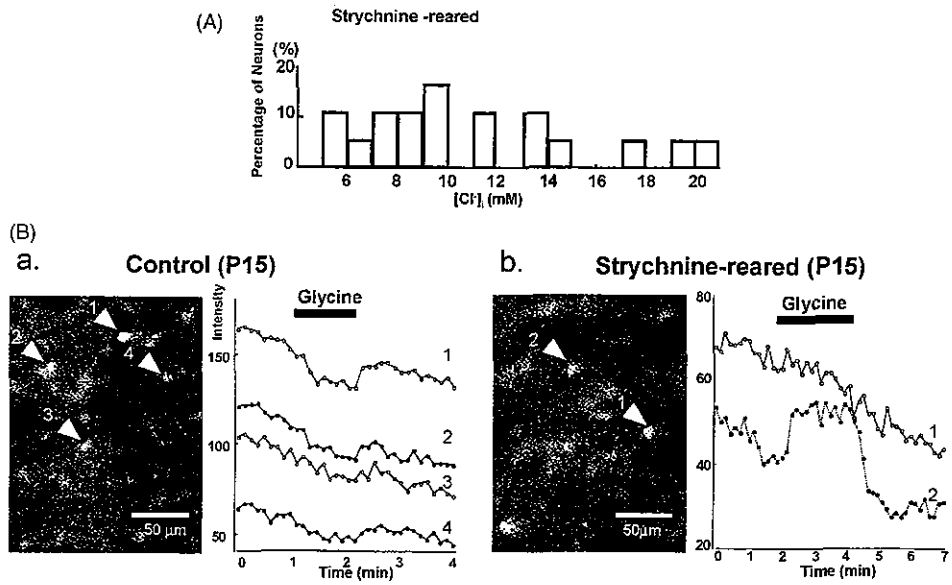

Fig. 5. Strychnine-reared rats maintain a high intracellular Cl^-. (A) Distribution of $[Cl^-]_i$ in neurons from P14–P16 rats in which strychnine pellets were implanted subcutaneously at a posterior mid-dorsal location at P3. Note the greater number of neurons with high $[Cl^-]_i$ (11.1 ± 1.1 mM, $n = 18$) than in the cochlear ablated experimental groups (Figs. 4 and 5A). (B) Effects of glycine on MEQ fluorescence in neurons from control (a) and strychnine-reared (b) rats. A decrease in fluorescence indicates an increase of $[Cl^-]_i$ and occurs in response to glycine in sham-operated control rat neurons (a). In contrast, in some neurons from strychnine-reared rats, there was an increase in fluorescence (i.e., a decrease in $[Cl^-]_i$) due to their higher resting $[Cl^-]_i$ (b).

KCC2 mRNA expression in the cytoplasmic constituents harvested from the same cell.

In three LSO neurons isolated from P0–P2 rats, KCC2 mRNA expression was only detected in the cell with the lowest $[Cl^-]_i$, which was about 14 mM (Fig. 6). All three neurons isolated from P14–P16 rats had $[Cl^-]_i$ about 10 mM or less, and all showed clear KCC2 mRNA expression (Fig. 6). We also performed combined RT-PCR and $[Cl^-]_i$ measurements on single LSO neurons isolated from P14–P16 rats with previous cochlear ablations. In two neurons that had received bilateral cochlea ablations, $[Cl^-]_i$ was maintained at a relatively high value and no KCC2 mRNA expression was observed (Fig. 6). In neurons from P14–P15 rats which had received either ipsilateral or contralateral ablations at P7, there was a good correlation between KCC2 mRNA expression and $[Cl^-]_i$, with only those neurons with $[Cl^-]_i$ below about 15 mM showing any KCC2 mRNA expression. This result suggests that activity in auditory afferents leads to an up-regulation of KCC2 expression, causing increased K^+-dependent Cl^- extrusion and a developmental decrease in $[Cl^-]_i$.

4. Discussion

In the present study, we have confirmed that there is a developmental decrease in $[Cl^-]_i$ in LSO neurons, and that this change is promoted by auditory-experience and seems to involve, at least partly, activation of glycine receptors.

4.1. Developmental changes of $[Cl^-]_i$ and Cl^- regulators

In many immature neurons, $GABA_A$ and glycine receptor-mediated responses are depolarizing and excitatory, and this is due to a high $[Cl^-]_i$ in immature neurons. While a developmental decrease in $[Cl^-]_i$ has been widely

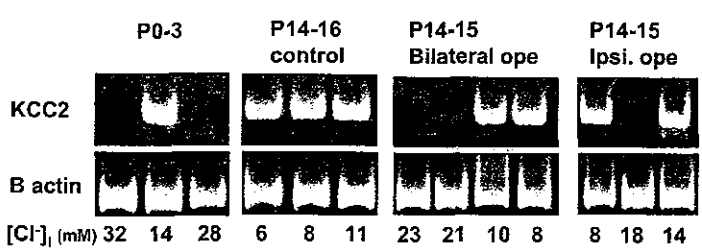

Fig. 6. KCC2 mRNA expression in single LSO neurons. Relationship between $[Cl^-]_i$ and the presence of KCC2 transcripts in individual LSO neurons from P0–P3 rats (left panel), from control P14–P16 rats (second panel from left) and from P14–P16 rats with previous cochlea ablations (right panels). KCC2 mRNA expression by single-cell RT-PCR was correlated with $[Cl^-]_i$ from the same cell. For LSO from P0–P3 rats, and for rats with previous bilateral, contralateral or ipsilateral ablations, KCC2 mRNA expression was only observed in those neurons in which $[Cl^-]_i$ was quite high. KCC2 expression was robust in all P14–P16 control neurons. β-Actin was expressed in all neurons.

reported in neurons, there is not complete consensus as to the underlying mechanisms, and particularly how KCC contributes. In the hippocampus, an up-regulation of KCC2 mRNA correlates well with the developmental decrease in $[Cl^-]_i$ (Rivera et al., 1999; Gulyas et al., 2001). Developmental increases in KCC2 expression levels have also been reported for the rat neocortex (Clayton et al., 1998; DeFazio et al., 2000) and the rat retina (Vu et al., 2000). Conversely, KCC2 expression levels are down-regulated following axotomy (Nabekura et al., 2002) and seizures (Reid et al., 2001); both of these events are also associated with increases in $[Cl^-]_i$. Difference in the levels of KCC2 expression between motor neurons and sensory neurons are also well correlated with their $[Cl^-]_i$ (Ueno et al., 2002). Hence a number of studies support an increase in KCC2 expression levels as a significant cause of developmental, pathological and random variations in neuronal $[Cl^-]_i$. On the other hand, however, KCC2 is reported to be already expressed in immature hippocampal neurons (Kelsch et al., 2001), in inferior colliculus neurons (Vale et al., 2003) and in LSO neuron (Balakrishnan et al., 2003) although, for reasons not yet clear, it does not seem to function effectively in extruding Cl^- at this developmental stage (see also Fig. 1, Kakazu et al., 1999). Our results suggest that KCC2 mRNA levels are too low to detect in many neonatal LSO neurons but becomes detectable in all neurons by 2 weeks after birth, a time when $[Cl^-]_i$ is reduced (Fig. 6A). Our results also indicate some heterogeneity in the developmental changes in Cl^- homeostasis, with KCC2 expression and low $[Cl^-]_i$ being observed in some neonatal neurons (Fig. 1).

Several reports indicate that neuronal activity is involved in the developmental and pathological regulation of Cl^-. In cultured hippocampal neurons, activation of $GABA_A$ receptors, but not glutamate receptor activation, promotes the increase in KCC2 mRNA expression and the associated decrease in $[Cl^-]_i$ (Ganguly et al., 2001). Deafferentation of gerbil inferior colliculus neurons (by bilateral cochlea ablation) at least partially prevents the typical developmental shift in the equilibrium potential of IPSCs to more hyperpolarized potentials (Vale and Sanes, 2000). The relatively depolarized IPSC reversal potential in the ablated gerbils was due to a lack of Cl^- transport function rather than any change in expression levels of KCC2 or NKCC1 (Vale et al., 2003). In our experiments, bilateral cochlear ablation also disrupted the normal developmental change in $[Cl^-]_i$, this is likely to be due to reduced LSO neuronal activity. Prior to the onset of hearing (which occurs around P10–P12 in rats), activation of Cl^- channels induces neuronal depolarization in the LSO (Kandler and Friauf, 1995), due to the high $[Cl^-]_i$ (Kakazu et al., 1999; Ehrlich et al., 1999). Our results are consistent with the hypothesis that this depolarizing afferent input, and the resulting membrane depolarization, are important in the development of KCC2 expression and Cl^- homeostasis. A similar disruption to Cl^- regulation was observed with either chronic strychnine treatment, ipsilateral ablation (causing predominantly a loss of glutamatergic afferents) or contralateral ablation (causing loss of GABAergic/glycinergic afferents). This suggests that both neurotransmitter systems can contribute to the changes in $[Cl^-]_i$, possibly reflecting their common ability to excite LSO neurons. Alternatively, ipsilateral ablation might also indirectly reduce GABAergic/glycinergic inputs to the LSO neurons, e.g., by decreasing excitatory input to local interneurons. This would be more consistent with the observation that activation of $GABA_A$ receptors, but not glutamate receptors, contributes to enhanced KCC2 expression (Ganguly et al., 2001).

4.2. Changes in the auditory brain stem with development

The LSO receives excitatory projections driven by sound input into the ipsilateral ear, and inhibitory projections driven by the contralateral ear. We show here that these inputs are required for development of Cl^- homeostasis. While this may be associated with inhibitory synaptic transmission, a number of other changes are occurring around the time when rats and gerbils acquire hearing ability (between P10 and P14). During the first 2 weeks after birth, massive synapse remodeling takes place within the LSO that is associated with changes in both morphology and function. Around the onset of hearing, there is a refinement of inhibitory afferent arborizations and the LSO dendrites that they innervate (Sanes and Friauf, 2000), including elimination of GABAergic/glycinergic inhibitory inputs (Kim and Kandler, 2003) and a change in the nature of the major inhibitory neurotransmitter from GABA to glycine (Kotak et al., 1998).

Several reports also suggest a role for afferent activity in these developmental changes. Removing the cochlear in the first neonatal week disturbs these refinements of axonal and dendritic morphology at inhibitory synapses (Sanes et al., 1992; Sanes and Chokshi, 1992). Contralateral cochlear ablation in immature gerbils, as well as in vivo application of strychnine, disturbs the refinement of dendritic spread of LSO neurons (Sanes and Takacs, 1993).

Our present study provides evidence that another crucial change in LSO physiology, i.e., alterations in Cl^- regulation, is also dependent on hearing experience. Sound afferents from the both the ipsilateral and contralateral ears are important in the maturation of $[Cl^-]_i$ homeostasis in LSO neurons, possibly due to their common depolarizing effect.

Acknowledgements

The authors wish to thank Dr. Andrew Moorhouse for language-editing this manuscript. This work was supported by Grants from the Ministry of Education, Science and Culture, Japan (Nos. 15016082, 15650076 and 15390065) to J.N.